Brd4 as a candidate protein for the recognition of histone H3 lysine 27 acetylation

Ingvild Stensland

The thesis is submitted in partial fulfillment of the requirements for the degree of Master of Science

Department of Molecular Biology

Faculty of Mathematics and Natural Sciences

University of Bergen

2015

Acknowledgements

The work presented in this master thesis was carried out at the Department of Molecular Biology, University of Bergen, in the period January 2014 to June 2015, in the NucReg research program. The supervisor was Rein Aasland, and co-supervisor Signe Värv.

First, I would like to thank my supervisor Rein Aasland, for encouragement, insightful advice and guidance.

I would also like to thank my wonderful co-supervisor Signe Värv, for helping me with anything and everything. You have gone far and beyond to help me with my experiments and with my writing. Also, thank you for all the buffers and solutions you let me “borrow”.

A big thanks goes out to Kirill Jefimov, for always having a contagiously good mood. It is impossible to feel down near you, keep it up.

I also want to thank Øyvind Strømland for helping me with ITC, DLS and SEC experiments. I shall raise a statue in your honor.

I would also like to thank everyone in Nucreg for helping out, and especially Diana Turcu for help with the Biacore.

Thank you Fredrik for supporting me.

Table of Contents

Abbreviations

- BD1- Bromodomain 1 of Brd4
- BD2- bromodomain 2 of Brd4
- BET family- Bromodomain and extraterminal-domain family
- Brd4- Bromodomain containing protein 4
- Btn- Biotin moiety
- ChIP- Chromatin immunoprecipitation
- DLS- Dynamic light scattering
- GST- Glutathione S-transferase
- PTM- Post-translational modification
- H3K27ac- Acetylation mark on lysine 27 in histone H3
- H3K4me1- Mono-methylation mark on lysine 4 in histone H3
- H3K4me3- Tri-methylation mark on lysine 4 in histone H3
- H4tera-ac- Acetylation marks on lysines 5,8,12, and 16 in histone H4
- HAT- Histone acetyl-transferase
- HDAC- Histone deacetylase
- IMAC- Immobilized metal affinity chromatography
- IPTG- Isopropyl β-D-1-thiogalactopyranoside
- ITC- Isothermal titration calorimetry
- NPS- Region of N-terminal clusters of phosphorylation sites in Brd4
- NRC- Nucleosome remodeling complex
- Pdi- Polydispersity index (Reported from DLS)
- PIC- Preinitiation complex
- Pol II- RNA polymerase II
- P-TEFb- Positive transcription elongation factor b
- SEC- Size exclusion chromatography
- SILAC- Stable isotope labeling of amino acids in cell culture
- SPR- Surface plasmon resonance

Abstract

Post-translational modifications (PTMs) of histone tails are associated with the regulation of transcriptional processes. Patterns of histone modifications mark regions of high or low transcriptional activity, and are recognized by “reader proteins”. The reader proteins are often transcription factors that recruit chromatin remodelling complexes or enzymes that add further modifications to histone tails.

Genomic enhancer regions, responsible for cell-type specific activation of different genes, have been found to exhibit distinct patterns of histone modifications. Active enhancers are enriched in acetylation of histone H3 lysine 27 (H3K27ac), a mark which distinguishes active from poised and primed enhancers. In this work, we wished to find a protein which specifically recognizes this histone modification.

Bromodomain- containing protein 4 (Brd4) is a transcriptional regulator that is known to be involved in the regulation of elongation by RNA polymerase II (Pol II). Brd4 has been shown to co-localize with H3K27ac at active enhancers, and was therefore chosen as a candidate for selective recognition of H3K27ac.

Possible binding between the two bromodomains of Brd4 and H3K27ac was investigated by histone peptide binding assays, isothermal titration calorimetry (ITC) and surface plasmon resonance (SPR). Brd4 bromodomain constructs containing one or both bromodomains were engineered, and proteins were expressed and used in binding assays. Strong binding between Brd4 bromodomain 1 (BD1) and a H4 peptide acetylated at four lysines (H4tetra-ac) was observed, but in contrast to a previously published study, no binding between either of the Brd4 bromodomains to H3K27ac was detected in histone peptide binding assays and ITC.

Possible reasons for these discrepancies are discussed and alternative functions for Brd4 and its bromodomains at enhancer and promoter regions are suggested.

1. Introduction

Eukaryotic multicellular organisms such as mammals contain a multitude of different cell types that have varying morphology, size and function. All the diverse tissues of a grown human, from a well-toned bicep muscle to the epithelia lining the intestines, come from one single cell; the fertilized egg. They all contain the same genetic material on DNA level hence holding the same information for protein synthesis, yet they display very distinct phenotypes.

In multicellular organisms, differences between cell types are determined by differences in their gene-expression profiles, which are represented by the types and amounts of proteins and RNA that are present in each cell. Regulation of protein production mainly takes place at the transcription level, where the binding and activation of RNA polymerase II (PoI II) at the transcription start site determines if a gene is transcribed or not. The association of Pol II at the start of a protein-coding region is determined by its recognition of sequence elements within the gene known as promoters. A promoter is a regulatory DNA element that is commonly located close to the coding region. Binding and activation of Pol II at the promoter is mediated by transcription factors and co-activators, proteins that guide and load the polymerase to the promoter, and release it from its promoter-proximal pausing.

Comparative genome analyses have revealed that the complexity of organisms does not correlate with increased gene number, and relies more on the refinement of gene expression regulation. Just under 20,200 protein-coding genes have so far been identified in the human genome (UniProtKB, June 2015), which is more than in the fruit fly *Drosophila melanogaster,* but less than in the common grape or the plant *Arabidopsis thaliana* (Pertea and Salzberg, 2010). While the number of genes in the human genome is rather low, the estimated number of regulatory DNA sequences is in the range of several hundred thousand (Dunham et al., 2012). In eukaryotic cells, and especially in multicellular organism, the regulation of transcription by the promoter alone is not enough, and an interplay of different regulatory elements, such as silencers, insulators and enhancers is needed. In addition, a further level of regulation is imposed on the genome at the level of chromatin packing, and through the deposition of post-translational modifications (PTMs) on DNA-binding proteins called histones (Cheung et

al., 2000). A multitude of such modifications exist, and the pattern of different modifications in different genome regions has been found to correlate with gene expression and repression.

1.1 Structure of chromatin and the nucleosome

The packaging of eukaryotic DNA has important consequences for the availability of the genes within it. Tightly packed DNA is less accessible as a template for transcription, and thus transcriptional activators do not only interact with the transcriptional machinery, but they also regulate transcription through inducing changes in DNA packaging.

In eukaryotic cells, long stretches of DNA are managed by coiling them around histone proteins, to form a structure know as a nucleosome. Two copies of each of four core histones, H2A, H2B, H3 and H4, form an octamer around which 147 bp of DNA is wrapped (Luger et al., 1997) (Figure 1.1). Linker DNA, bound by the linker histone H1, serve to join the nucleosomes together, forming a structure commonly described as resembling beads on a string. Histones are small globular proteins with unstructured N- or C-terminal "tails". They have a high degree of positive charge due to a high content of lysine and arginine residues. Electrostatic interactions between the negatively charged phosphate backbone of DNA and the many positive amide groups of the histones contribute to the tight binding between histones and DNA. The formation of nucleosomes allows the DNA to take on folded conformations that reduce its linear length, which is vital to fit the DNA into the nucleus in an organized manner.

The nucleosome is the basic structural and functional unit of chromatin; a dynamic fiber of nucleosomes and non-histone proteins. Chromatin can be packed into higher-order structures, mainly depending on the stage of the cell cycle. In metaphase, before cell division occurs, the chromatin is packed tightly into chromosomes to equally partition the DNA into both daughter cells, but during interphase its structure is more loose and open, allowing RNA polymerases to transcribe genes (Raynaud et al., 2014). However, little is known about how higher-order chromatin structures are formed. The local structures of chromatin during interphase can be divided into two types; euchromatin and heterochromatin. Actively transcribed genes are found in euchromatin, while regions that

are transcriptionally silent, such as telomers and centromers, are found in the more compact and inaccessible heterochromatin (Grewal and Jia, 2007).

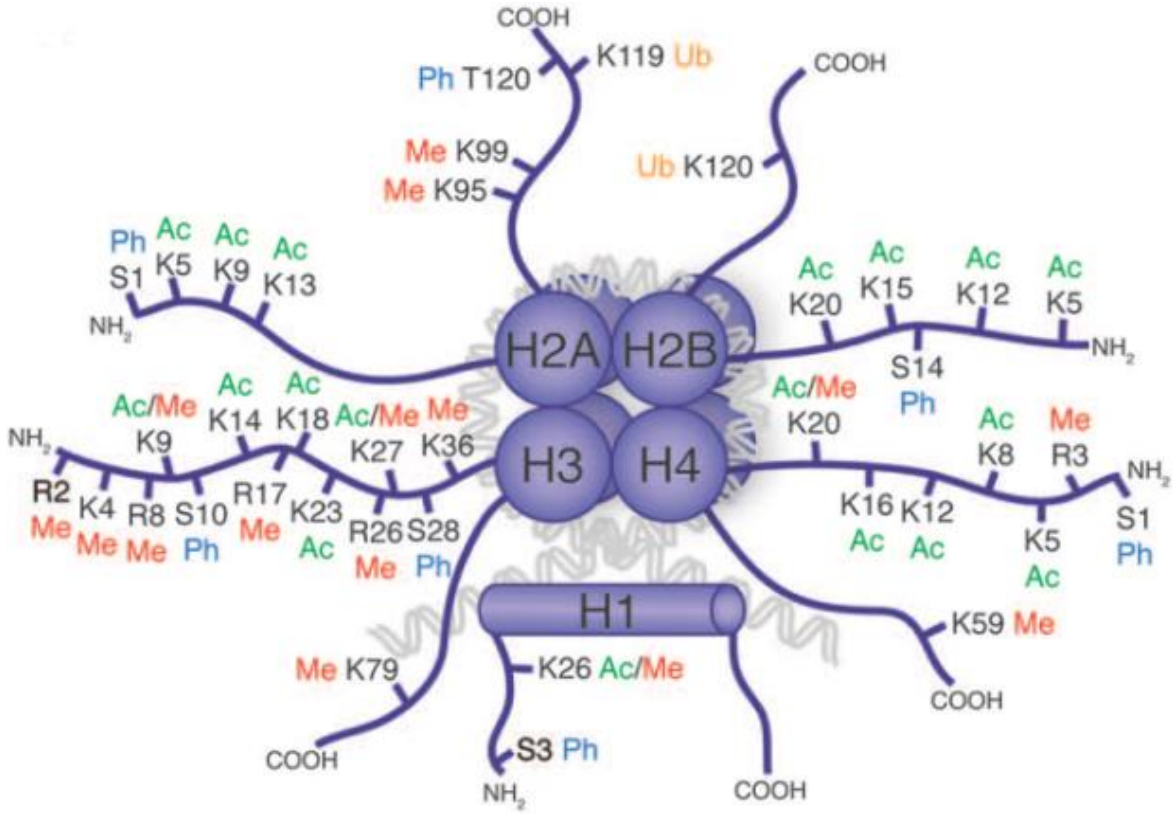

Figure 1.1: Nucleosome with a selection of post-translational modifications on histone C-(COOH) and N-(NH_2) terminal tails. PTMs placed on histone tails: Ac:-Acetyl; Me-Methyl; Ph-Phosphoryl; Ub-Ubiquitin. Numbers and upper case letters indicate amino acid residues as follows: K-lysine; T-threonine; S-serine; R-arginine. DNA wrapped around the core histones is shown in light grey. (Perla Cota, 2013)

The packaging of DNA into nucleosomes and chromatin limits the accessibility of the DNA, making it less available for proteins involved in transcription and replication. To allow transcription to occur, nucleosomes must be disrupted and the histones displaced. Post-translational modification of the protruding N-terminal tails of histone proteins have been shown to influence the accessibility of nearby DNA region, both through disruptions in contacts between nucleosomes, and through the recruitment of proteins with enzymatic functions (Kouzarides, 2007).

1.2 Histone post-translational modifications

The idea that specific patterns of PTMs on histone proteins can influence gene expression is part of the field of epigenetics. The term epigenetics has changed over the years, and is still subject of debate. Therefore an operational definition of epigenetics introduced by Berger *et al.* is used in this thesis: "An epigenetic trait is a stably heritable phenotype resulting in changes in a chromosome without alterations in the DNA sequence" (Berger et al., 2009). Histone PTMs, are thought to constitute an epigenetic "histone code" (Strahl and Allis, 2000), which is passed down to daughter cells and influences which genes should be active, and which should be repressed in a specific cell type. In this way the modifications provide a way to maintain cellular identity throughout several cell divisions (Armstrong, 2014). The PTMs placed on histone tails are often referred to as histone marks.

To date, at least fifteen types of histone PTMs have been identified at 130 different sites on the core histone proteins and linker histone (Sadakierska-Chudy and Filip, 2014). Some report even higher numbers of possible histone modifications (Tan et al., 2011). Histone PTMs are reversible, and are placed on histone tails by histone modification enzymes often called "writers" of the histone code, and removed by "erasers". The most widespread and studied histone modifications are acetylation, methylation and phosphorylation (Figure 1.1). Acetylation occurs on lysine residues, while methylation is found as mono-, di- or trimethyl on lysines, and as mono- or di-methyl on arginines (Kouzarides, 2007). Phosphorylations are found on serine, threonine and tyrosine residues (Oki et al., 2007). Among other common PTMs are ubiquitination (Zhang, 2003) and sumoylation (Shiio and Eisenman, 2003).

The vast array of possible modifications gives a wide potential for different responses, as the marks serve as signaling platforms that govern interactions between chromatin and proteins involved in transcription (Strahl and Allis, 2000). Acetylation of lysine residues in histone tails has been found to correlate with regions of high gene activity (Grunstein, 1997), while methylation is found in both active and repressed regions. Lysine trimethylation (Kme3) at histone H3 lysine 4 (H3K4), H3K36 and H3K79 are enriched in gene-coding regions and are involved in gene expression (Kouzarides, 2000; Strahl et al., 1999). Methylation of H3K9 and H3K27, however, are associated with repression of gene expression, and are found in heterochromatin and heterochromatin-boundary regions

(Trojer and Reinberg, 2007). Actively transcribed regions are marked by hyper-acetylation of histones H3 and H4, which is thought to disrupt the chromatin structure and allow transcriptional factors to access the DNA (Struhl, 1998). The addition of an acetyl group on a lysine residue removes the positive charge of the ε- nitrogen (Figure 1.2), which can decrease the net positive charge of the basic histone tails and thus decrease its electrostatic interactions with the negative DNA backbone, and to other nucleosomes (Kouzarides, 2000). Acetylation marks are placed on lysines by the action of histone acetyltransferases/lysine acetyltransferases (HATs/KATs) and removed by histone deacetylases (HDACs) (Shahbazian and Grunstein, 2007). Proteins recruited to histone modifications bind though specific domains which are often termed as "readers" of the histone code. Different modifications recruit a different set of proteins which have diverse functions on chromatin composition and gene expression of nearby genomic regions. Histone acetylations are non-randomly placed in chromatin, and particular marks, such as H3K27ac are enriched in specific genomic regions, such as promoters and enhancers.

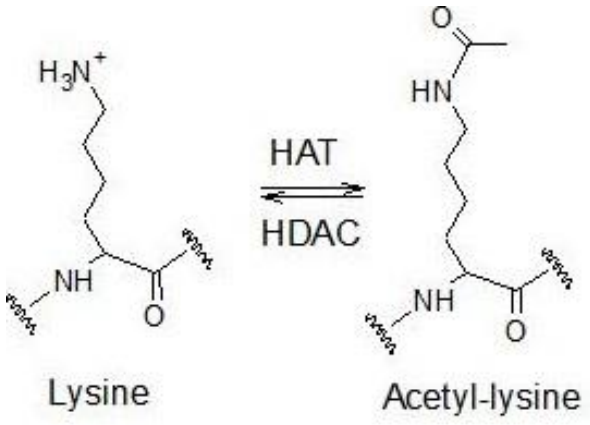

Figure 1.2: Chemical structures of lysine and acetyl-lysine. Acetylation of lysine residues happens through the placement of an acetyl-group on the ε-nitrogen by the actions of histone acetyltransferases (HATs), and is removed by histone deacetylases (HDACs). Waved lines represent connections to the rest of the polypeptide chain.

1.3 Enhancers

The differences between cell types arise from differential gene expression. Some genes are actively transcribed in one cell-line, but repressed in another and *vice versa*. In metazoans, the regulation of transcription is not only limited to the promoter region, but is distributed among a complex set of distal regulatory sequence elements. Enhancers are one class of such regulatory elements and have been found to be the major determinant of cell type specificity (Bulger and Groudine, 2010; Heintzman et al., 2009). Enhancers are defined as DNA sequence elements that when linked *in cis* to a promoter, can increase its

activity regardless of orientation. The properties of enhancer elements were first described for a viral SV40 sequence that enhanced the transcription of a hemoglobin β1 gene introduced into HeLa cells, (Banerji et al., 1981). Target promoters can be located thousands of base pairs either upstream of downstream from the enhancers that control them, and he median distance between enhancer and promoter has been estimated to be 125 kb, with the majority of enhancers being located within 500 kb of the promoter they regulate (Jin et al., 2013). There are however examples of enhancers that act from even longer distances (Amano et al., 2009).

Enhancers are comprised of clusters of recognition sequences for cell-specific transcription factors, and are typically a few hundred base pairs in length. Enhancers, as well as other regulatory elements, exhibit hypersensitivity for DNaseI digestion. This sensitivity has been attributed to the exclusion of nucleosomes in the enhancer region, due to binding of transcription factors, which increases DNA accessibility at particular sites (Elgin, 1988). Studies of genome-wide DNaseI hypersensitivity and transcription factor binding sites have suggested that a large portion of enhancers are cell-type specific (Xi et al., 2007), and that only a small fraction are active in any given cell line. This is consistent with their role as determinants of cell type-specific gene expression. The ENCODE consortium has identified approximately 400,000 enhancer-like elements in the human genome (Dunham et al., 2012), while the FANTOM consortium has reported 43,000 active enhancer candidates (Andersson et al., 2014). Active enhancers increase transcription of genes by interacting with its paired promoter. The mechanisms of how this occurs are however still very much under debate. The current view is that enhancers influence promoter activity through direct encounters in three-dimensional space, through the action of DNA-looping (Figure 1.3) (Bulger and Groudine, 1999). The enhancer brings several needed transcription factors and co-activators to the promoter, which in turn either promote assembly of the preinitiation complex (PIC) at the promoter, or release of the paused Pol II downstream of the promoter which drives the transition from initiation to elongation (Plank and Dean, 2014). Promoters that are engaged in looping have been shown to have significantly increased levels of transcription (Rao et al., 2014). Interestingly, studies in *Drosophila* have revealed that three-dimensional interactions between enhancers and promoters do not change during development,

which indicates that transcription is activated by additional signals after DNA looping has brought the enhancer and promoter into proximity of each other (Ghavi-Helm et al., 2014). This type of pre-existing loops have also been observed in mouse and human cells (Jin et al., 2013; de Laat and Duboule, 2013). In the light of these findings, one hypothesis of how enhancer-mediated gene expression is activated is that after enhancer –promoter looping, Pol II is recruited but paused downstream of the promoter. The recruitment of transcription factors, or even possibly additional enhancers then triggers the pause-release of Pol II, which promotes elongation (Ghavi-Helm et al., 2014).

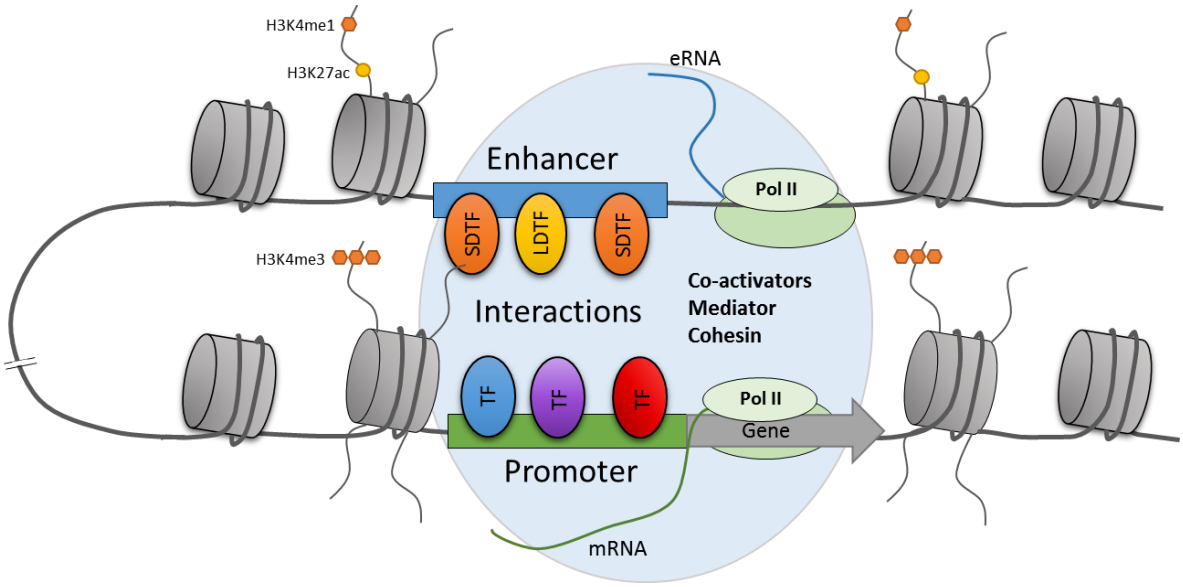

Figure 1.3: Enhancer-promoter interactions. Enhancers interact with their cognate promoters through direct interactions facilitated by DNA looping. Enhancers are activated by the binding of linage-dependent (LDTF) and- signal-dependent (SDTF) transcription factors, and the presence of an acetyl modification on histone H3 lysine 27 (H3K27ac). Enhancers are marked by monomethylation of lysine 4 (H3K4me1), while promoters are found to exhibit trimethylation of lysine 4 (H3K4Me3). Elongation by Pol II occurs at both active enhancers and promoters. For simplicity, only one Pol II is shown.

Enhancers have been found to be able to control more than one gene, and recent studies have indicated that active enhancers interact with approximately two promoters on average, while active promoters were found to have contacts with 4-5 enhancer-like elements on average (Jin et al., 2013). These findings suggest that it is the combinatorial control of several enhancers on a promoter that determines a gene's expression in a specific cell type. Most enhancer-promoter interactions occur in distinct chromatin domains known as topological association domains (Dixon et al., 2012). These domains on average contain 5-10 genes and a few hundred enhancers (Jin et al., 2013). Even though

information about enhancer-promoter interactions is accumulating, an important question still remains unanswered; how do enhancers interact with their cognate promoters specifically, and what proteins are involved in these interactions?

1.4 Histone modifications and enhancer activation

Genome wide studies have suggested that enhancers exhibit a characteristic chromatin signature in the form of histone PTMs and also specific transcription factor binding. The modifications that are displayed can be used to distinguish between different enhancer states (Ernst and Kellis, 2010). Enhancer states can be classified as inactive, primed, poised or active. Inactive enhancers, buried in compact chromatin, are not bound by transcription factors and show no typical pattern of histone modifications. Primed enhancers are bound by lineage dependent sequence-specific transcription factors, making them ready for subsequent activation by binding of signal dependent factors (Ernst and Kellis, 2010). Primed enhancer regions are marked by histone H3 lysine 4 mono-methylation (H3K4me1) and di-methylation (H3K4me2) (Heintzman et al., 2007). Poised enhancers are similar to primed enhancers, but are in addition marked with a repressive H3K27me3 mark (Rada-Iglesias et al., 2011). In poised enhancers, histone deacetylase (HDAC)- containing complexes maintain histones in a repressed deacetylated state, while nucleosome remodeling complexes (NRCs) keep the region nucleosome-free (Reviewed in Heinz et al., 2015). Methyltransferases which maintain H3K4 and H3K27 methyaltion are also present at poised enhancers. The poised state is most commonly found in embryonic stem cells, and is located near key early developmental genes (Rada-Iglesias et al., 2011).

Active enhancers share many of the features of poised enhancers, but are able to drive gene expression. Acetylation, rather than trimethyaltion of H3K27 is one of the hallmarks of active enhancers (Creyghton et al., 2010), and is placed on histone H3 by the HAT p300 and CREB-binding protein CBP (Tie et al., 2009). Poised enhancers become active during differentiation, when the trimethyaltion mark (H3K27me3) is exchanged for the acetylation mark H3K27ac (Rada-Iglesias et al., 2011). Other important features associated with active enhancers is the presence of actively transcribing Pol II in the company of the Mediator complex (de Santa et al., 2010). Pol II transcription at active

enhancers is bidirectional, and produces enhancer RNA (eRNA). eRNAs are short RNA sequences that are not spliced, and have short half-lives (Kim et al., 2010). Pol II recruitment to enhancers and changes in eRNA expression are highly correlated with the expression of nearby genes, suggesting that the transcription of eRNA at enhancers is important for enhancer function (Reviewed in Lam et al., 2014) .

The available evidence suggests that enhancers are marked with H3K4me1 as a general mark priming them for activation, and that further modification with H3K27ac distinguish them as active (Rada-Iglesias et al., 2011). The presence of H3K4me1 is not unique to enhancers, and is also found in 5' portions of transcribed genes, and in broad regions around enhancer elements (Calo and Wysocka, 2013). Its presence is, however, often found to precede nucleosome depletion, and deposition of H3K27ac. Acetylation of H3K27 is almost exclusively found in regions that have already been marked by H3K4me1 (Bonn et al., 2012), adding weight to the hypothesis that H3K4me1 primes enhancers for later activation. It is important to note that H3K27 acetylation is not exclusive to enhancers, as active promoters are also found to exhibit this mark (Shlyueva et al., 2014). Although chromatin signatures can be used to identify enhancer position and activity, direct evidence showing the role of enhancer chromatin modifications *in vivo* is still lacking.

Finding a protein that specifically recognizes the H3K27 acetylation mark might cast some light on how this modification contributes to the activation of enhancers, and to subsequent enhancer-facilitated gene transcription.

1.5 Acetylation- recognition domains

The most well-known acetyl-lysine recognition domain is the bromodomain. The human genome encodes 61 bromodomains in 46 different proteins. Many bromodomain-containing proteins are multi-modular and can harbor catalytic domains, protein-interaction domains and even more than one bromodomain. (Filippakopoulos et al. 2012). Although there are large sequence variations among different bromodomains, they all share a conserved fold of a left-handed bundle of four α- helices linked by loop regions of variable length (Figure 1.4.A). The helices are denoted α_Z, α_A, α_B, α_C, while the linking loop regions are named ZA and BC. The long loop between helices α_Z and α_A, (the ZA loop) is

packed together with a loop connecting α_B and α_C (BC loop) to form a deep hydrophobic pocket at one end of the four-helix bundle (Figure 1.4.B). (Dhalluin et al., 1999) It is this hydrophobic cavity that binds the acetyl-lysine side chain through hydrogen bonding to a conserved asparagine located in the BC loop. Only a small number of lysine acetylation marks have been identified to specifically interact with individual bromodomains, and they often exhibit low affinities (Filippakopoulos et al., 2012).

Bromodomains were long thought to be the only domains able to specifically recognize acetyl-lysine motifs, but recently other domains have been found to exhibit specificity to acetyl-lysine histone marks as well. Some tandem plant homeodomain (PHD) zinc fingers, and the plecstrin-homology (PH) domain of yeast chaperone protein Rtt106 have been shown to bind histone H3 in an acetylation-sensitive manner (Ali et al., 2012; Su et al., 2012). A newly discovered domain called YEATS, named after its five founding domain-containing proteins Yaf9, ENL, AF9, Taf4 and Sas5, has also been reported to bind acetyl-lysine modifications (Li et al., 2014). The YEATS domain of AF9, a component of the super elongation complex (SEC) was found to bind acetylated histone H3, with a preference for H3K9 acetylation. The affinity of AF9 YEATS binding to H3K9ac was found to be much higher than that of many bromodomains (Li et al., 2014).

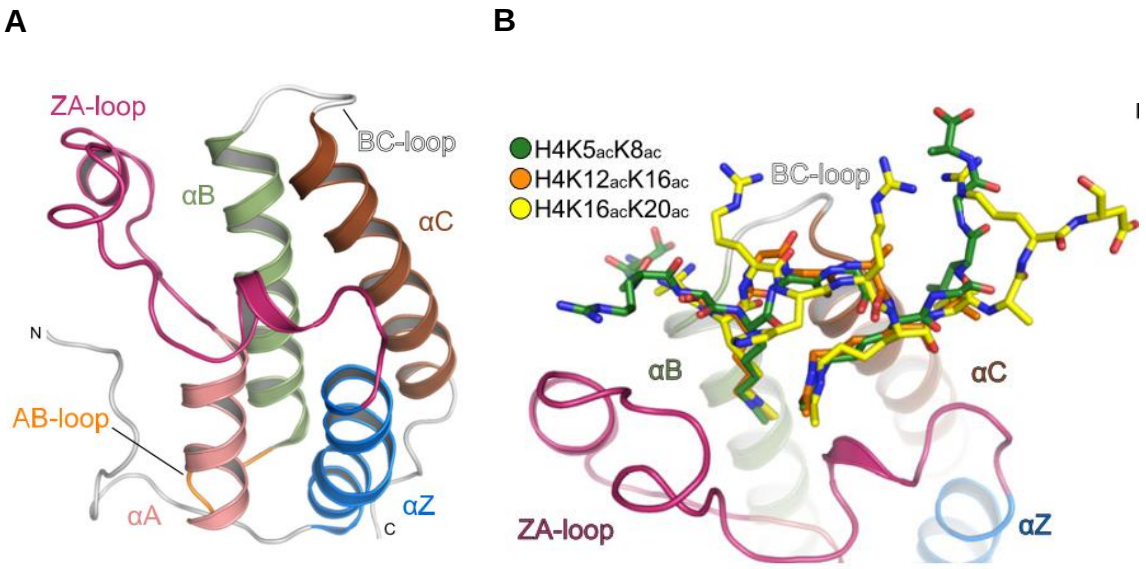

Figure 1.4: Three dimensional structure of bromodomain 1 (BD1) of Brd4. A: The conserved bromodomain fold of Brd4 bromodomain 1. **B:** The ZA and BC loops are packed together to form a hydrophobic binding pocked for acetyl-lysine. The figure shows an overlay of three doubly acetylated histone peptides bound in the hydrophobic pocked. (Filippakopoulos et al. 2012)

1.6 Bromodomain containing protein 4 (Brd4)

Brd4 is a bromodomain containing protein that is part of the bromodomain and extraterminal domain (BET) family. The BET family is conserved from yeast to mammals, and includes mammalian Brd2, Brd3, Brd4 and BrdT. The BET proteins are adaptor proteins that are involved in in the regulation of transcription by Pol II (Florence and Faller, 2001). The BET proteins all contain two N-terminal bromodomains, BD1 and BD2, which recognize acetylated lysine residues on histone tails and other proteins (Figure 1.5). They also contain a conserved and unique extraterminal domain (ET-domain) which is involved in interactions with proteins such as histone modifiers and NRCs (Liu et al., 2013; Rahman et al., 2011). The bromodomains of the BET-family are highly conserved, and share similar hydrophobic binding pockets for the binding of acetylated lysines. The two bromodomains, BD1 and BD2, however exhibit less similarity within the same protein than to their homologous domains in other BET-family members (44% to 75% identity) (Nakamura et al., 2007). Brd4 is the most widely studied of the BET- proteins, as it is a therapeutic target in several cancers (Shi and Vakoc, 2014). Brd4 is ubiquitously expressed in mammals, and knockout of Brd4 in mice has been shown to lead to early embryonic lethality (Houzelstein et al., 2002).

Three distinct human Brd4 isoforms have been identified, A, B and C. The three differ only in the C-terminal region (CTD), where isoforms B and C either completely lack this region (B) or have a shorter unique version (C). Isoform A, hereafter referred to as Brd4, is involved in transcription by Pol II, through interactions with different proteins and complexes, such as the mediator complex (Wu and Chiang, 2007), and the positive transcription elongation factor b (P-TEFb) (Moon et al., 2005). P-TEFb is a dimer of the cyclin dependent kinase Cdk9 and one of its regulatory subunits cyclin T1, T2 or K. This complex promotes transcriptional elongation by Pol II by releasing it from its pausing at the promoter-proximal region through phosphorylation of Pol II's C-terminal domain, and of Pol II-associated negative regulatory factors (Peng et al., 1998). P-TEFb is under tight regulation, and the majority of inactive P-TEFb is sequestered in a small ribonucloprotein complex, which represses its kinase activity (Prasanth et al., 2010). Brd4 binds to P-TEFb through a two-pronged binding, where a P-TEFb interaction domain (PID) in its C-terminal region binds to Cdk9, while the second bromodomain, BD2, binds a set of

acetylated lysine residues in cyclin T1. (Schröder et al., 2012). Brd4-binding to P-TEFb releases it from its repressive factors, and recruits it to promoter regions in a bromodomain-mediated fashion (Figure 1.6). (Moon et al., 2005). Less is known about Brd4's interactions with the Mediator complex, but the two have been shown to occupy many of the same regions across the genome (Lovén et al., 2013). In addition, the first identification of Brd4 was with the original purification of the human Mediator complex (Jiang et al., 1998).

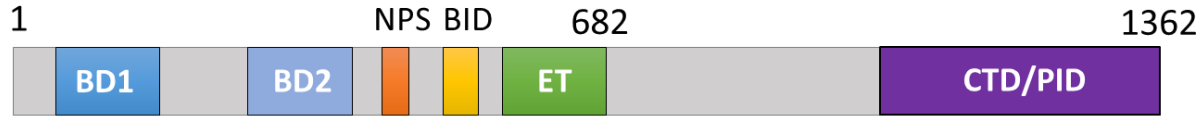

Figure 1.5: Brd4 domain organization. Brd4 is a 1362 amino acids long protein with two N-terminal bromodomains, BD1 and BD2, an extraterminal domain (ET) and a C-terminal P-TEFb interaction domain (CTD/PID). In addition, it has an N-terminal cluster of phosphorylation sites (NPS) which is important in its regulation, and a basic residue enriched interaction domain (BID).

Brd4 has also been implicated in activation of transcription independently from P-TEFb, through the recruitment of NSD3, a histone methyltransferase that methylates H3K36; a modification enriched in transcriptionally active regions (Rahman et al., 2011). This recruitment occurs through the ET domain of Brd4.

Chromatin immunoprecipitation coupled with DNA- sequencing (ChiP-seq) has been utilized to analyze the genome-wide chromatin occupancy of Brd4. In agreement with its role as a transcriptional regulator, Brd4 has been found at essentially all active promoters, but also at a significant portion of active enhancers in various normal and transformed cell types (Lovén et al., 2013; Zhang et al., 2012). In these types of experiments, active enhancer regions are defined by their enrichment of H3K4me1 and H3K27ac, an acetylation mark that as described above, is one of the hallmarks of active enhancers. Particularly high Brd4-occupancy is found in large clustered enhancers called super-enhancers, where the level of H3K27ac is higher than in typical enhancers (Lovén et al., 2013). Super-enhancers regulate the expression of cell-fate determining genes, and are bound by high levels of master transcription factors and the Mediator complex (Whyte et al., 2013). While Brd2 and Brd3, other BET-family proteins, are found mostly at promoters, higher levels of Brd4 are found at a selection of enhancers than at promoters (Engelen et al., 2015).

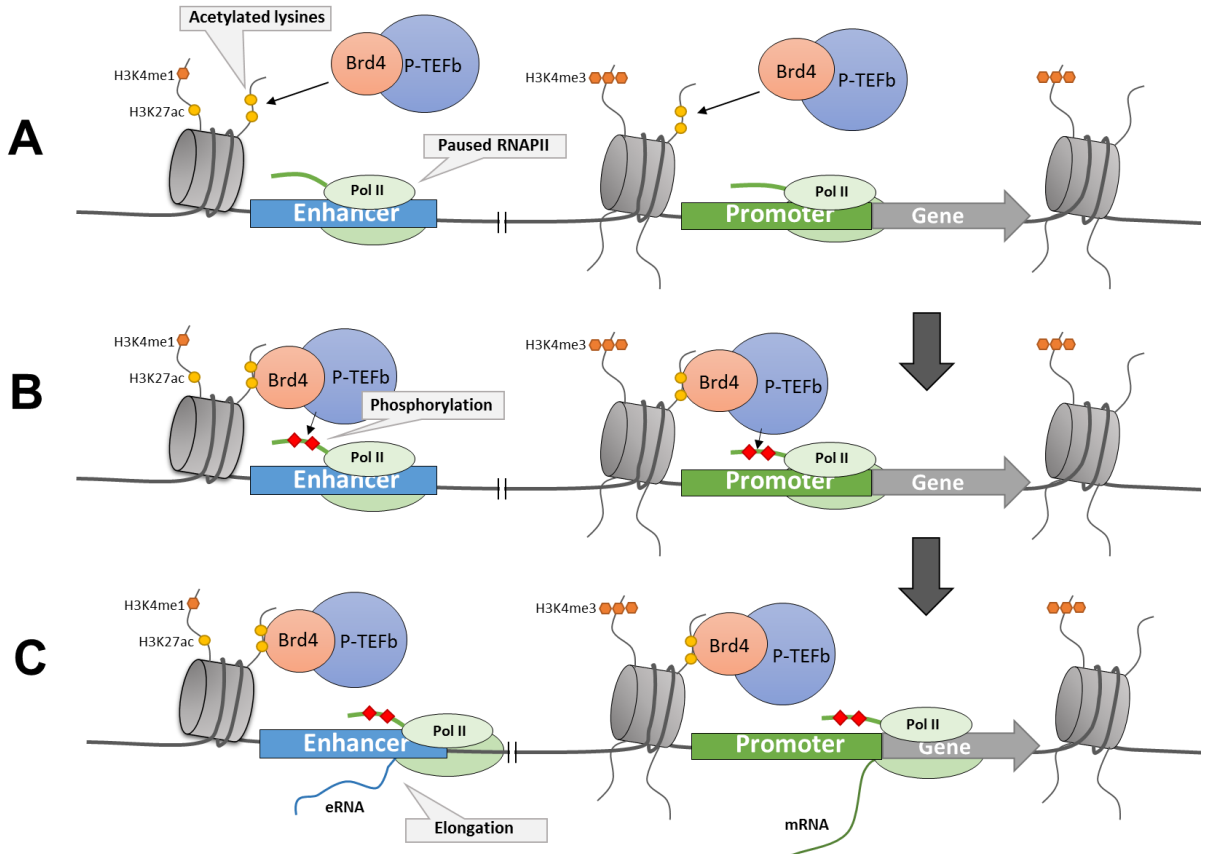

Figure 1.6: Model of Brd4-mediated Pol II pause-release. A: Brd4 binds to P-TEFb through its P-TEFb interaction domain, PID, and recruits it to acetylated chromatin at enhancers and promoters. Brd4 binds acetylated lysines on histone H3 and H4 tails. **B:** The kinase component of P-TEFb phosphorylates serine residues in the C-terminal tail of Pol II, and negative factors bound to Pol II (not shown). **C:** Phosphorylation of the CTD and removal of negative factors leads to pause-release of Pol II, which continues the elongation of eRNA at enhancers, and mRNA at gene bodies. Only one Pol II is shown for transcription at enhancers and promoters.

Brd4 has been found to facilitate elongation of eRNA at enhancers in a manner that is bromodomain-dependent. This was discovered when the addition of JQ1, a specific BET-bromodomain inhibitor, was found to antagonize eRNA synthesis at Brd4-associated enhancers (Kanno et al., 2014). Evidence has also been put forth suggesting that Brd4 interacts with the arginine demethylase Jmjd6 and P-TEFb to regulate pause-release of Pol II at a large number of genes. This is proposed to occur through the binding of Brd4 and Jmjd6 to distal anti-pause enhancers leading to the release of paused Pol II at cognate promoters through looping and interactions with P-TEFb (Liu et al., 2013).

As it has been suggested that Brd4 is recruited to enhancers in a manner dependent on its bromodomains, and that it has been found to co-localize with H3K27ac, Brd4 arises as a candidate for H3K27ac recognition.

1.7 Aim and strategy of the study

Our research group is investigating the role of histone acetylation in enhancer function and, in particular, the role of H3K27ac which is enriched in enhancer chromatin. While others in the group are searching for H3K27ac-binding proteins by pull-down experiments and mass-spectrometry, the purpose of this project has been to investigate Brd4 as a candidate H3K27ac-binding protein. It had been previously reported that Brd4 co-localize with H3K27ac marks in enhancer chromatin (Lovén et al., 2013). Furthermore, a medium through-put SPOT assay with all human bromodomains had identified BD1 of Brd4 as a candidate H3K27ac-binder (Filippakopoulos et al., 2012).

On this basis, the aim of this study has been to confirm the binding between Brd4 BD1 and H3K27ac with quantitative methods and prepare for further functional studies.

Three in vitro binding assays were chosen for this work: i) histone peptide binding assays, which would give information of binding specificity; ii) ITC and iii) SPR which would both give quantitative information of the affinity of binding.

2. Materials

Table 2.1: Chemicals

Name	Abbreviation/formula	Supplier
2-[4-(2-hydroxyethyl)piperazin-1-yl]ethanesulfonic acid	HEPES	Sigma Life Science
Acrylamide/Bis-acrylamide 37.5:1 (30%)	$C_3H_5NO/C_7H_{10}N_2O_2$	Sigma Life Science
Ammonium persulfate	APS	Merck
Ampicillin	Amp	Bristol-Myers Squibb
Agar-agar		Merck
Agarose		Sigma L.S
Boric acid	H_3BO_3	Merck
Bovine serum albumin	BSA	Sigma
Bromophenol blue	BPB	Sigma
Calcium chloride	$CaCl_2$	Merck
Chloroform	$CHCl_3$	Sigma
Deoxyribonucleotide triphosphate (ATP, TTP, CTP, GTP)	dNTPs	Takara
Dimethyl sulfoxide	DMSO	Sigma
Dithiothreitol	DTT	Sigma
Disodium hydrogen phosphate	$Na_2HPO_4 \bullet 2H2O$	Merck
EDTA-free protease inhibitor cocktail		Roche Diagnostics
Ethanol	EtOH	Kemethyl
Ethidium bromide	EtBr	Sigma
Ethylenediaminetetraacetic acid	EDTA	Merck
Glycerol	$C_3H_4O_3$	Sigma-Aldrich
Hydrochloric acid	HCl	Sigma-Aldrich
Imidazole (1H-Imidazole)	$C_3H_4N_2$	Merck

Isopropyl β-D-1-thiogalacto-pyranoside	IPTG	VWR
Magnesium chloride	$MgCl_2$	Merck
Methanol	MetOH/ CH_4O	Sigma-Aldrich
N,N,N′,N′-Tetramethylethane-1,2-diamine	TEMED	Sigma-Aldrich
Nonidet P40, nonycphenyl-polyethylene glycol	NP-40	Sigma-Aldrich
Peptone		Merck
Polyethylene sorbitan monolaurate	Tween® 20	Sigma-Aldrich
Potassium chloride	KCl	Merck
Skimmed milk powder		Merck
Sodium acetate	CH_3COONa	Merck
Sodium chloride	NaCl	Sigma-Aldrich
Sodium dodecyl sulfate	SDS	Bio-Rad
Sodium hydroxide	NaOH	Merck
Tris(2-carboxyethyl)phosphine	TCEP	Thermo Scientific
Tris(hydroxymethyl)amino-methane hydrochlorid	Tris-HCl	Sigma-Aldrich
Triton X-100	$(C_2H_4O)_4C_{14}H_{220}$	Sigma
Yeast extract		Merck

Table 2.2: Pre-prepared commercial buffers and reagents

Name	Purpose	Supplier
Imperial™ Protein Stain	SDS-PAAG staining	Thermo Scientific
BigDye® v.3.1	DNA sequencing	Applied Biosystems
Running gel buffer (1 M Tris-HCl pH 8.8)	SDS-PAAG	Bio-Rad
Stracking gel buffer (0.5 M Tris-HCl pH 6.8)	SDS-PAAG	Bio-Rad
TG, Transfer buffer	Immunoblotting	Bio-Rad
TGS, Running buffer	SDS-PAGE	Bio-Rad
TRI Reagent® Trizol	RNA extraction	Sigma Life Science

Table 2.3: Antibodies, source and working dilutions

Name	Origin	Dilution	Type	Supplier
Anti-GST	Rabbit	1:10,000	Polyclonal	Sigma
ECL Anti-rabbit (HRP-conjugated)	Donkey	1:10,000	Secondary	GE Healthcare

Table 2.4: Bacterial strains

Strain	Purpose	Supplier
Escherichia coli BL12-CodonPlus®-RIL	Protein expression	Agilent
Escherichia coli M15	Protein expression	Sigma-Aldrich
Escherichia coli XL1-blue	DNA amplification	Agilent

Table 2.5: Commercial kits

Kit	Use	Supplier
Amersham ECL Plus Western Blotting Detection Reagents	Immunoblot detection	GE healthcare
Nucleospin® Gel and PCR clean-up	DNA purification	Macherey-Nagel
Nucleospin® Plasmid	Miniprep plasmid purification	Macherey-Nagel
Nucleobond® Xtra Midi	Midiprep plasmid purification	Macherey-Nagel

Table 2.6: Enzymes for cDNA syntehsis and cloning

Name	Supplier
Go-Taq flexi polymerase	Promega
Phusion™ Hot Start II DNA Polymerase	Thermo Scientific
M-MuLV reverse transcriptase	Thermo Scientific
T4 DNA ligase	New England Biolabs

Table 2.7: Plasmids

Name	Antibiotic resistance	Protein product tag	Reference/supplier
pSXG	Ampicillin	N-terminal GST	Ragvin *et al*., 2004
pQE30	Ampicillin	N-terminal 6x His	Qiagen
pSXG-p300B (HUMAN_EP300, 1039-1196)	Ampicillin	N-terminal GST	Ragvin *et al*., 2004

Table 2.8: Protein molecular weight and DNA size markers

Name	Purpose	Supplier
2-log DNA ladder	DNA size marker	New England Biolabs
Precision Plus Protein Dual Color Standard	Protein size marker	Bio-Rad

Table 2.9: Restriction enzymes

Name	Recognition sequence and cleavage site	Supplier
BamHI	5’ G|GATCC 3’	Takara
EcoRI	5’ G|AATTC 3’	Takara
HindIII	5’ A|AGCTT 3’	Takara

Table 2.10: Consumables

Name	Purpose	Supplier
PD-10 desalting column	Buffer exchange	GE Healthcare
PVDF Hybond-P membranes	Immunoblotting	Amersham
Slide-A-Lyzer® Dialysis cassettes (3.500 MWCO)	Dialysis	Thermo Scientific
Slide-A-Lyzer® MINI units (3.500 MWCO)	Dialysis	Thermo Scientific

Table 2.11: Resins used for protein purification and peptide binding assays

Name	Purpose	Supplier
Glutathione Sepharose 4B resin	GST-protein purification	GE Healthcare
Ni-NTA agarose resin	IMAC purification	Qiagen GmbH
Streptavidin Sepharose™ high performance	Histone peptide pulldowns	GE Healthcare

Table 2.12: DNA primers

Primer	Primer sequence, 5'-3'	Purpose
BRD4-FL-F	ATAGGATCCTATCTGCGGAGAGCGGCCCT	Cloning
BRD4-FL-R	ATACCTAGGCGCTCAGAAAAGATTTTCTTCAAAT	Cloning
BD1-pSXG-F	AATTAGAATTCAACCCCCCGCCCCCAG	Cloning
BD1-pSXG-R	AATGGATCCTCATTCTTCTGTGGGTAGCTCATTTATTTTTTG	Cloning
BD2-pSXG-F	AATTAGAATTCAAGGACGTGCCCGACTCTC	Cloning
BD2-pSXG-R	AATGGATCCTCACTCGTCCGGCATCTTGGC	Cloning
BD1-pQE30-F	AATGGATCCAACCCCCCGCCCCCAG	Cloning
BD1-pQE30-R	AATAAAGCTTTCATTCTTCTGTGGGTAGCTCATTTATTTTTTG	Cloning
BD2-pQE30-F	AATGGATCCAAGGACGTGCCCGACTCTC	Cloning
BD2-pQE30-R	AATAAAGCTTTCACTCGTCCGGCATCTTGGC	Cloning
BD1-s-F	AATTAGAATTCGTGCTCAAGACACTATGGAAAC	Cloning
BD1-s-R	AATGGATCCTTAAGCTTCTGCCATTAAGACTATGT	Cloning
BD2-s-F	AATTAGAATTCCGAGATGTTTGCCAAGAAGCACG	Cloning
BD2-s-R	AATGGATCCTTACTTGCGGGCCATGGCCAC	Cloning

BD1-seq-F	CCCCCAGAGACCTCCAAC	Sequencing
BD1-seq-R	AGCTTTCATTCTGTGGGTAGCTC	Sequencing
BD2-seq-F	AAGGACGTGCCCGACTCTCA	Sequencing
BD2-seq-R	CTCGTCCGGCATCTTGGCAAA	Sequencing
3PGEX	CCGGGAGCTGCATGTGTCAGAGG	Sequencing
5PGEX	GGGCTGGCAAGCCACGTTTGGTG	Sequencing
pQE30-seq-F	AGGCCCTTTCGTCTTCACCTC	Sequencing
pQE30-seq-R	CCATAAAAAACGCCCGGCGG	Sequencing

Table 2.13: Peptides for ITC from LifeTein

Name	Sequence	Modification	Extinction coefficient* (M^{-1} cm^{-1})	M.W (Da)
H3K27ac	APRKQLATKAAR(Kac)SAPATG GVKY	Lys(Ac)	1490	2412.84
H4tetra-ac (H4K5,K8, K12,K16ac)	SGRG(Kac)GG(Kac)GLG (Kac)GGA(Kac)RKVLRDNY	4*Lys(Ac)	1490	2628.04

*Calculated with the online resource ProtParam

Table 2.14: Biotinylated peptides for histone peptide binding assays from Biosyntan

Name	Sequence	Modification	M.W (Da)
H3(15-36)-Btn	APRKQLATKAARKSAPATGGVK-EDA-Btn	None	2475.7
H3K27-Btn	APRKQLATKAAR(Kac)SAPATGGVK-EDA-Btn	Lys(Ac)	2517.7
H3K23-Btn	APRKQLAT(Kac)AARKSAPATGGVK-EDA-Btn	Lys(Ac)	2518.9
H3K23acK27ac-Btn	APRKQLAT(Kac)AAR(Kac)SAPATGGVK-EDA-Btn	2*Lys(Ac)	2560.9
H3K27me1-Btn	ATKAAR(Kme1)SAPATGGVKKPHRYRPG-GK-Btn	Lys(Me1)	2931.5
H4 (2-24)-Btn	SGRGKGGKGLGKGGAKRHRKVLRGSGSK-Btn	None	3005.0
H4tetra-ac-Btn	SGRG(Kac)GG(Kac)GLG(Kac)GGA(Kac)R-HRKVL-EDA-Btn	4*Lys(Ac)	2641.9

Table 2.15: Instruments and equipment

Name	Use	Manufacturer
Allegra X-15 R Centrifuge	Centrifugation	Beckman Coulter
Avanti J-26 XP Centrifuge	Centrifugation	Beckman Coulter
Biacore T100, T200 sensitivity enhanced	Surface plasmon resonance	Biacore (GE Healthcare)
ChemiDoc™ XRS+	Immunoblot imaging	Bio-Rad
GelDoc™ EZ	Gel imaging	Bio-Rad
Nano ITC	Isothermal titration calorimetry	TA Instruments
Trans-Blot® Turbo™	Immunobloting	Bio-Rad
Zetasizer Nano ZS	Dynamic light scattering	Malvern
Zen2112 quartz cuvette	Dynamic light scattering	Malvern
Ækta explorer	Size-exclusion chromatography	GE Healthcare
Superdex 75 HiLoad™ prepgrade 16/600 colum	Size-exclusion chromatography	GE Healthcare

Table 2.16: Software

Name	Use	Developer/Website
Biacore T200 Control Software v.2	SPR experiment control	Biacore (GE Healthcare)
Biacore T200 Evaluation Softwave v.1	SPR data analysis	Biacore (GE Healthcare)
Clustal Omega	Multiple sequence alignment	http://www.ebi.ac.uk/Tools/msa/clustalo/
Imagelab v	SDS-gel and immunoblot visualization	Bio-Rad
ITCRun v.2	ITC experiment control	TA Instruments
NanoAnlayze v2.4.1	ITC data analysis	TA Instruments
ND-1000	Protein/DNA concentration determination	Saveen-Werner

OligoCalc	Oligo Tm calculator	http://www.basic.northwestern.edu/biotools/oligocalc.html
ProtParam	Protein parameters	http://web.expasy.org/protparam/
SnapGene® Viewer v.2.7.3	Generation of plasmid maps	GSL Biotech LLC
Unicorn 5.2	Äkta control software	GE Healthcare

2.1 Prepared buffers and solutions

2.1.1: Solutions for agarose gel electrophoresis

Table 2.17: TBE buffer

Chemicals	Concentrations
Tris base	100 mM
Boric acid	90 mM
EDTA	1 mM

Table 2.18: 6x DNA loading buffer

Chemicals	Concentrations
Tris-HCl	10 mM
Bromophenol blue	0.03% (w/v)
Glycerol	60% (v/v)
EDTA	60 mM

Table 2.19: Agarose gel

Chemicals	Concentrations
Agarose in 0.5x TBE	1-2 % (w/v)
Ethidium bromide	0.5 µg/ml

2.1.2 Media for cultivation of bacteria

Table 2.20: Lysogeny Broth (LB medium)

Chemicals	Concentrations
Tryptone	10 g/l
NaCl	10 g/l
Yeast extract	5 g/l

Table 2.21: LB-agar

Chemicals	Concentrations
Tryptone	10 g/l
NaCl	10 g/l
Yeast extract	5 g/l

Agar	15 g/l

2.1.3 Buffers and solutions for SDS-PAGE and immunoblotting

Table 2.22: SDS- polyacrylamide resolving gel

Components	Final Concentrations	Stock solution
Acrylamide/bisacrylamide	12-15% (w/v)	30%, 37.5:1
Tris-HCl pH 8.8	390 mM	1.5 M pH 8.8
SDS	0.1% (w/v)	20% (w/v)
APS	0.1% (w/v)	10% (w/v)
TEMED	0.04 % (v/v)	99% (v/v)

Table 2.23: SDS-Polyacrylamide stacking gel

Components	Final Concentrations	Stock solution
Acrylamide/bisacrylamide	3.4% (w/v)	30%, 37.5:1
Tris-HCl pH 6.8	172 mM	0.5 M pH 6.8
SDS	0.1% (w/v)	20% (w/v)
APS	0.1% (w/v)	10% (w/v)
TEMED	0.08% (w/v)	99% (v/v)

Table 2.24: 1x SDS running buffer

Chemicals	Concentrations
Tris-HCl pH 8.3	25 mM
Glycine	192 mM
SDS	0.1 % (w/v)

Made from 10x TGS and TG commercial buffers

Table 2.25: 1x Transfer buffer

Chemicals	Concentrations
Tris-HCl pH 8.3	25 mM
Glycine	192 mM
Methanol	20 % (v/v)

Table 2.26: 2x SDS sample buffer

Chemicals	Concentrations
Tris-HCl pH 6.8	100 mM
SDS	4% (w/v)
Glycerol	20% (v/v)
DTT	200 mM
Bromophenol blue	0.2% (w/v)

Table 2.27: 1x PBS (tween)

Chemicals	Concentrations
Nacl	137 mM
KCl	2.7 mM
Na_2HPO_4	4.3 mM
KH_2PO_4	1.47 mM
(Tween-20)	(0.05 %)

2.1.4 Buffers and solutions for GST- fusion protein purification

Table 2.28: GST-purification lysis buffer

Components	Concentrations
Tris-HCl pH 7.5	250 mM
NaCl	50 mM
DTT	1 mM
Triton x-100	0.1 (v/v)
Protease inhibitor cocktail	1x

Table 2.29: Glutathione elution buffer

Chemicals	Concentrations
Reduced Glutathione	15 µM
Tris-HCl pH 8.0	50 mM

2.1.5 Buffers and solutions for IMAC protein purification

Table 2.30: IMAC lysis buffer

Chemicals	Concentrations
Tris-HCl pH 7.0	50 mM
NaCl	300 mM
Imidazole	20 mM
Triton-x 100	0.2 % (v/v)
EDTA free protease inhibitor	1x
DTT	1 mM

Table 2.31: IMAC wash buffer

Chemicals	Concentrations
Tris-HCl pH 7.0	50 mM
NaCl	300 mM
Imidazole	20 mM
DTT	1 mM

Table 2.32: IMAC elution buffer

Chemicals	Concentrations
Tris-HCl pH 7.0	50 mM
NaCl	300 mM
Imidazole	500 mM
DTT	1 mM

2.1.6 Buffers for protein- peptide binding studies

Table 2.33: Shi buffer

Chemicals	Concentrations
Tris-HCl pH 7.5	50 mM
NaCl	300 mM
NP-40	0.1 % (v/v)
Protease inhibitor cocktail	1x

Table 2.34: ITC T7.5/T8.5 buffer

Chemicals	Concentrations
Tris-HCl pH 7.5/8.5	50 mM
NaCl	150 mM
TCEP	1 mM

3. Methods

3.1 Construction of expression vectors for Brd4 bromodomains

3.1.1 Primer design

Primers were designed for amplification of the two bromodomains of human Brd4, BD1 and BD2 separately and together. Primers for two different sets of Brd4 constructs were created, one set which included only the core bromodomain sequences with five flanking residues on either side (BD1-s/BD2-s), and one where BET-family-specific flanking sequences were included (BD2/BD2) (Refer to figure 4.1 for construct sequences). Domain boundaries were based on sequences retrieved from UniProtKB (BRD4_HUMAN). Primers were designed with restriction sites for cloning into two different vectors, pSXG and pQE30 (Appendix 1). Sequencing primers specific for the Brd4 bromodomains and the pQE30 vector were also designed (Table 2.12). The online resource OligoCalc was used to calculate the melting temperature of designed primers.

The pSXG vector has an integrated N-terminal Glutathione S-transferase (GST) coding sequence, which upon expression produces a GST-tagged fusion protein. The fusion proteins can be purified with affinity chromatography. Inclusion of a GST tag can also improve the solubility of recombinant proteins. pQE30 encodes six N-terminal histidines (His-tag). His-tagged proteins can be purified through immobilized metal affinity chromatography (IMAC).

3.1.2 RNA extraction and cDNA synthesis

Total RNA was extracted from HeLa S3 cells using the trizol TRI Reagent®. A HeLa cell pellet from two 80% confluent 10 cm plates was homogenized by pipetting and incubation for 5 min at RT in 1 ml TRI Reagent®. 0.2 ml chloroform was added to the homogenized sample, and the solution was incubated for 3 min, before centrifugation at 12 000 g for 10 min. The upper aqueous phase was collected, and the RNA was purified by precipitation with 0.5 ml 100% isopropanol. The RNA pellet was washed with 1 ml 75% ethanol, air dried and resuspended in 30 µl RNase-free water. To achieve greater purity, RNA was subjected to ethanol precipitation with 0.1 volume of 3 M sodium acetate

pH 5.2 and 2.2 volumes 100% ethanol at -20 °C for 20 min. The RNA pellet was washed with 70% ethanol, air dried and dissolved in 50 µl RNase-free water.

First-strand cDNA synthesis from total RNA was performed with M-MuLV reverse transcriptase and oligo(dT) oligomers. A sample of 0.5-1 µg total RNA was mixed with 0.5 µg oligo(dT), 1X RT reaction buffer, 10 mM dNTPs, 40 U M-MuLV reverse transcriptase and dH_2O to a final volume of 25 µl. The reaction took place at 37 °C for 60 minutes, and was stopped by heat inactivation of the enzyme at 70 °C for 10 min.

3.1.3 PCR amplification of Brd4 bromodomains

PCR was carried out with cDNA template prepared as described above, and primers shown in table 2.12.

Table 3.1: Thermocycler program for the amplification of Brd4 bromodomains

Step	Temperature	Time	Cycles
Initial denaturation	98 °C	5 minutes	1
Denaturation	98 °C	10 seconds	
Annealing	Tm	30 seconds	30
Elongation	72 °C	1 minute	
Final elongation	72 °C	5 minutes	1

PCR was performed as shown in table 3.1, in 50 a µl reaction volume with final concentrations of 1X phusion HF reaction buffer, 200 µM dNTPs, 0.5 µM primers, 1 µl template cDNA, 3% DMSO and 0.02 U/µl Phusion™ Hot Start II DNA Polymerase.

3.1.4 Cloning of Brd4 bromodomains into expression vectors

PCR products were purified from agarose gel using NucleoSpin® Gel and PCR Clean-Up Kit from, following the manufacturer's instructions. A 1% agarose gel was used for the purification of BD2 and BD1+BD2 PCR products, while a 2% gel was used for purification of BD1. The purified PCR products were subjected to restriction digestion by appropriate restriction enzyme. The pSXG vector and the PCR products to be inserted in it were digested with BamHI and EcoRI, while pQE30 and its inserts were digested with BamHI and HindIII. PCR product digestion was carried out as a double digestion in a 50 µl

reaction volume with 1X buffer K, 0.3 U/µl restriction enzymes and 10 ng/µl insert DNA. The reaction was carried out at 37 ° for one hour, and stopped by heat inactivation at 70 °C for 10 minutes. The digested DNA inserts were purified using Nucleospin® Gel and PCR clean-up column. pSXG and pQE30 plasmids were linearized by restriction in a 50 µl reaction with 1X buffer K, 0.6 U/µl restriction enzymes (pSXG: BamHI/EcoRI, pQE30:BamHI/HindIII) and 40 ng/µl plasmid DNA. The reaction was carried out at 37 °C for 3 hours. The digested plasmids were purified from a 1% agarose gel using a Nucleospin® Gel and PCR clean-up column. Concentrations of digested DNA inserts and plasmid vectors were determined using absorbance measurement at 260nm with NanoDrop.

The digested bromodomain DNA segments were inserted into the plasmid vectors pSXG and pQE30 by ligation with T4 ligase. Digestion with BamHI and EcoRI/HindIII left overhanging "sticky" bases on the inserts and vectors. The inserts were ligated into the vectors with a 1:3 vector to insert ratio. The amount of insert to be used for each reaction was determined using equation 3.1:

$$\frac{mass\ vector\ (ng) x\ length\ of\ insert\ (kb)}{length\ of\ vector\ (kb)}\ x\ molar\ ratio\ \frac{insert}{vector} = mass\ insert\ (ng) \qquad \text{Equation 3.1}$$

An amount of 100 ng vector was used in the ligation reactions. Ligations were carried out in a 20 µl reaction volume in 1X ligation buffer with 400 units T4 DNA ligase for 17 hours at 16 °C. The enzymes in the reaction were inactivated by heating to 65 °C for 10 minutes. An aliquot of 5 µl of the ligation reaction was used for heat-shock transformation with 50 µl chemically competent *E.coli* XL1-blue cells. Transformed cells were plated on LB agar plates with ampicillin for selection and growth. To check for successful ligation, colony PCR was performed in a 10 µl reaction with 1X GoTaq Flexi buffer, 2.5 mM $MgCl_2$, 0.8 µM forward and reverse sequencing primers (table 2.12), 0.2 mM dNTPs and 0,1 U/µl GoTaq® flexi DNA polymerase.

Table 3.2: Thermocycler program for colony- PCR

Step	Temperature	Time	Cycles
Initial denaturation	94 °C	5 minutes	1
Denaturation	95 °C	30 seconds	
Annealing	Tm	30 seconds	25
Elongation	72 °C	1 minute	
Final elongation	72 °C	5 minutes	1

3.1.5 Bromodmomain plasmid construct amplification and sequencing

Colonies that were expressing the ampicillin resistance gene were picked and grown in 5 ml LB mini-cultures with 100 µg/ml ampicillin for plasmid amplification, followed by mini-prep purification with NucleoSpin® Plasmid mini-prep kit. Plasmid constructs were sequenced in a 10 µl reaction containing, 150 to 300 ng of purified plasmid, 1 µl BigDye v.3.1, 1 µl sequencing buffer and 3,2 pmol of each primer. Cycle sequencing was carried out in a thermocycler with the program shown in table 3.3. After amplification, an additional 10 µl dH_2O was added to the reaction, and the samples were subjected to DNA sequencing at the in-house sequencing facility in a 3530xl DNA Analyzer from Applied Biosystems.

Table 3.3: Thermocycler program for DNA sequencing

Step	Temperature	Time	Cycles
Initial denaturation	96 °C	5 minutes	1
Denaturation	96 °C	10 seconds	
Annealing	55 °C	5 seconds	25
Elongation	60 °C	4 minutes	

Table 3.4 shows the name and description of bromodomain constructs that were made and verified by sequencing.

Table 3.4: Brd4 bromodomain constructs verified by DNA sequencing

Construct	Description*	Tag
pSXG-BD1	First bromodomain (BD1) of Brd4 in pSXG vector	N-terminal GST
pSXG-BD2	Second bromodomain (BD2) of Brd4 in pSXG vector	N-terminal GST
pSXG-BD1+BD2	First and second bromodomains of Brd4 in pSXG vector	N-terminal GST
pQE30-BD1	First bromodomain of Brd4 in pQE30 vector	N-terminal 6x His-tag
pQE30-BD2	Second bromodomain of Brd4 in pQE30 vector	N-terminal 6x His-tag
pQE30-BD1+BD2	First and second bromodomains of Brd4 in pQE30 vector	N-terminal 6x His-tag

*See figure 4.1 for details on bromodomain residues included in the constructs

3.2 Protein Expression and Purification

3.2.1 Expression of recombinant bromodomains

pSXG constructs (shown in table 3.4) were transformed by heat shock into chemically competent *E.coli* BL21-CodonPlus-RIL cells, while pQE30 constructs were transformed into *E.coli* M15 cells. Transformed bacteria were plated on LB-agar plates with ampicillin, and grown over night at 37 °C. Single colonies of transformed cells were picked and grown in 5ml LB mini- culture overnight at 37 °C with 100 µg/ml ampicillin. Start-up cultures were diluted in 750 ml fresh LB medium to an OD_{600} of 0.1. Expression of Brd4 bromodomain fusion proteins was accomplished by growth at 37 °C to an OD_{600} of 0.5, and then further growth at 18 °C until OD_{600} 0.8 was reached. Protein expression was induced by the addition of IPTG to a final concentration of 0.1 mM. Bacteria were harvested after roughly 16 hours by centrifugation at 8,700 x g for 15 min at 4 °C. Expression of GST and GST-p300B was induced by the addition of 0.4 mM IPTG after an

OD_{600} of 0.8 had been reached by growth at 37°C. Cells were harvested after 2 hours by centrifugation at 8,700 x g for 15 min at 4 °C.

Expression was verified using SDS-PAGE, as described in section 3.4.1. The theoretical parameters for expressed proteins are given in table 3.5.

Table 3.5: Theoretical parameters for expressed proteins*

Fusion protein	Theoretical molecular weight (kDa)	Theoretical extinction coefficient [M^{-1} cm^{-1}]	Theoretical pI
GST-BD1	42.6	69,790	6.68
GST-BD2	42.5	57,300	6.43
GST-BD1+BD2	74.7	84,230	8.74
GST	25.7	43,110	5.90
GST-p300B	41.3	70,040	6.36
His-BD1	16.3	27,055	8.49
His-BD2	16.0	14,440	7.17
His-BD1+BD2	48.3	41,370	9.16

*Calculated with ProtParam online resource

3.2.2 Purification of GST-fusion proteins

GST-fusion proteins were affinity-purified using glutathione Sepharose affinity purification resin. Bacterial pellets were washed in 40 ml PBS, and resuspended in 10 ml GST- purification lysis buffer per 1 g pellet wet-weight. Cells were lysed by sonication for 15 seconds at 60% intensity, with 30 seconds pauses, for a total sonication time of 2 minutes on ice. After sonication, 500 µl 20% Triton x-100 was added per 10 ml cell lysate, and incubated for 30 min at 4 °C. The cell lysate was centrifuged at 12 096 g for 6 minutes. The cleared supernatant was collected and 500 µl 50% glutathione Sepharose slurry was added. The cleared lysate was allowed to mix with the slurry on a soft shaker at 4 °C for 30 min. The slurry was collected by centrifugation at 2850 g for 6 min and washed twice with 5 ml cold GST-purification lysis buffer. Proteins were eluted by the addition of 400 µl glutathione elution buffer and incubation at 4 °C for 45 min. Eluates were collected by

1 minute centrifugation at 13,000 rpm in a tabletop minifuge. Eluted proteins were dialyzed GST-purification lysis buffer without protease inhibitor, overnight at 4 °C in Slide-A-Lyzer cassettes with 10.000 MW cutoff. The concentration of purified proteins was determined by absorbance measurements at 280 nm with NanoDrop. The online resource ProtParam was used to estimate the theoretical molecular weights and extinction coefficients of the GST- fusion bromodomains (Table 3.5). Protein purity was examined with SDS-PAGE, as described in section 3.4.1.

3.2.3 Purification of his-tagged proteins

His-tagged proteins were purified by immobilized metal affinity chromatography, using a Ni-NTA agarose column. Bacterial pellets were thawed on ice and resuspended in 10 ml IMAC lysis buffer per 1 g pellet. The bacterial suspension was incubated with 1 mg/ml lysozyme on ice for 20 minutes. Cells were lysed by sonication at 60 % intensity for 15 seconds with 30 second pauses to a total of 2 minutes. The lysate was centrifuged at 16,000 g for 20 minutes. The column was equilibrated by three column volumes of IMAC wash buffer. The cleared lysate was filtered through a 0.45 µm filter and allowed to flow through the column twice by gravity flow. A total of 5-15 column volumes (CV) of IMAC wash buffer was then added, before the protein was eluted with 2 CV of IMAC elution buffer. Protein concentration was measured with NanoDrop, while the purity was examined with SDS-PAGE as described in section 3.4.1.

3.3 Determining degree of protein aggregation

3.3.1 Size exclusion chromatography

Principle

Size exclusion chromatography (SEC) can be used to estimate the molecular weight of proteins. Separations of proteins by SEC is based on the Stokes radii. If a calibration curve of known proteins is constructed, the method can be used to estimate the molecular weight of an unknown protein. The standard curve is made by plotting the partition coefficients (K_{av}) of a series of standard proteins against the logarithm of their molecular weight. The partition coefficient describes the degree of interaction between a given size

exclusion media and an analyte for a given set of experimental parameters (Hong et al., 2012).The K_{av} is calculated using equation 3.2, where V_e is the elution volume for the protein, V_0 the column void volume and V_c the geometric column volume. The void volume is equal to the elution volume for the standard molecule Blue Dextran 2000, which is a large polymer of anhydroglucose with an approximate molecular weight of 2000 kDa. Because of its size, this polymer will be eluted prior to most other complexes and proteins. SEC can also be used to assess the oligomeric state of a protein.

$$K_{av} = \frac{V_e - V_0}{V_c - V_0} \qquad \text{Equation 3.2}$$

Execution

To determine the oligomeric state of purified His-tagged BD1, SEC was performed. His-BD1 was purified as described above, and 0.5 ml of 4 mg/ml (245 µM) was loaded on a 120 ml Superdex 75 prepgrade 16/600 column connected to an ÄKTA explorer FPLC system. The flowrate was set to 1 ml/min and elution was monitored by measuring absorbance at 280 nm. A standard curve was made from elution data of standard proteins which are presented in table 3.6. The standard proteins were analyzed under the same conditions as His-BD1. In order to determine the oligomeric status of His-BD1 The equation from the linear regression was used to calculate the molecular weight of his-BD1.

Table 3.6: SEC standard proteins

Protein	Molecular weight (kDa)
Albumin	66
Carbonic anhydrase	29
Lysozyme	14.3
Aprotinin	6.5

3.3.2 Dynamic light scattering

Principle

Dynamic light scattering (DLS) is a method for measuring the hydrodynamic size and size distribution of molecules and particles in solution or suspension. Laser light is directed into the sample, and the Brownian motion of particles in suspension causes the light to be scattered at different intensities. Analysis of these fluctuations yields the velocity of the Brownian motion, which is directly related to the particle's hydrodynamic radii (Wyatt Technology, 2015). The reported particle size parameter from a DLS experiment is the hydrodynamic diameter, defined as "the size of a hypothetical hard sphere that diffuses in the same fashion as that of the particle being measured" (Malvern Instruments 2011). The degree and rate of aggregation can be measured by DLS, by investigating whether the hydrodynamic diameter of the particle increases over time.

Execution

Particle sizes and degree of aggregation of the His-tagged Brd4 bromodomains were determined using DLS. After purification of His-BD1 and His-BD2, the buffer was exchanged to a 50 mM Tris-HCl, 150 mM NaCl, 1 mM DTT buffer at pH 7.5 using a PD-10 desalting column. Dynamic light scattering was measured at a protein concentration of 214 µM for His-BD1, and 131 µM for His-BD2. Before the measurement was conducted a standard operating procedure (SOP) was set up for size determination, and in the SOP the dispersant viscosity was set to reflect the buffer in use. Measurements were done in a Zen2112 quartz cuvette at 25 °C. The His-BD1 sample was centrifuged at 20 000 g for 10 min before measurements to remove insoluble material. Measurement of 280 µM lysozyme (14.3 kDa), a monomeric protein with similar molecular weight as His-BD1 and His-BD2, under the same conditions was used as a control. The rate of aggregation of His-BD1 was measured by reading the dynamic light scattering at 5 min intervals over a time course of 16 hours.

3.4 Histone peptide binding assay

Principle

In the histone peptide binding assay (Shi et al., 2006), the protein of interest is mixed with a short synthetic biotinylated peptide with desired modifications. A streptavidin-Sepharose resin is then added, and the biotinylated peptide will bind to it. If the protein of interest interacts with the peptide, it too will be retained on the Sepharose resin. After several steps of washing, the protein-peptide complexes are eluted from the resin, and the composition of the eluate is investigated by immunoblotting.

Execution

Several acetylated and unmodified histone peptides were used in the binding assay, and are listed table 2.14. Purified GST-fusion proteins were mixed with biotinylated histone peptides at a 0.1:1 µM ratio in 150 µl Shi buffer. This mix was incubated on a rotating wheel overnight at 4 °C. Aliquots of 15 µl streptavidin Sepharose slurry were added, and the samples were incubated at 4 ° for one hour on a rotating wheel. The samples were centrifuged at 1500 g for 2 min, and resin was washed four times with 200 µl Shi buffer, and two times with 200 µl 50 mM Tris-HCl pH 8.0. After washing, the resin was resuspended in 30 µl 2x SDS sample buffer and heated at 95 °C for 5 minutes. Aliquots of 10 µl of resuspended resin were analyzed by immunoblotting with anti-GST antibody.

3.4.1 SDS-PAGE

SDS-PAGE was carried out to separate proteins by molecular weight and for analysis with immunoblotting. The electrophoresis of GST-fusion domains was carried out in 12% polyacrylamide-SDS gels at 25 mA in 1x TGS buffer, while 15% gels were used for the smaller, his-tagged domains.

3.4.2 Immunoblotting

Immnunoblotting was used to detect proteins that had bound to biotinylated peptides in the histone peptide binding assay, and been separated with SDS-PAGE. The immunoblotting was carried out using polyvinylidene fluoride blotting membrane (PVDF). The blotting membrane was activated by treatment with 100% methanol for 5 seconds, followed by a 5 minutes wash with dH_2O. Membrane, polyacrylamide gel and blotting paper were equilibrated in cold transfer buffer for 10 min before blotting.

Transfer was performed in a Trans-Blot Turbo semi-dry transfer system for 20 min, 25 V, 1mA. After the transfer, the membrane was blocked with 5% skimmed milk in 1x PBS, 0.05% tween for 1 hour. After blocking, the membrane was incubated with polyclonal anti-GST antibody, at a 1:10,000 dilution in 5% skimmed milk PBS, 0.05% tween overnight at 4 °. The membrane was washed with PBS, 0.05% tween 4-6 times in 60 min (6 x 10 min) at room temperature before incubation with HRP-conjugated secondary antibody at 1:10,000 dilution for 1 hour in 5% skimmed milk, PBS, 0.05% tween. Secondary antibody was washed off with six washes with PBS, 0.05% tween. GST-antibody complexes were detected by 5 minutes incubation with ECL Prime western blotting reagent. Imaging of the membrane was conducted in a ChemiDoc XRS+ imaging system using ImageLab v.3.0.

3.5 Isothermal titration calorimetry

Principle

Isothermal titration calorimetry (ITC) is a method that can measure binding reaction parameters such as the strength of association, the stoichiometry and the thermodynamics of a reaction. It measures the heat that is released or consumed by stepwise titration of a ligand into a solution of the macromolecule/protein of interest. The strength of a binding reaction is usually expressed in the form of K_a, the association constant, or as the Gibbs free energy. In protein-ligand binding reactions, the dissociation constant, K_d, which is the inverse of K_a, is used to describe the affinity between a ligand and a protein. The stoichiometry of the binding reaction is represented by the symbol n, which gives the number of available binding sites per protein. The enthalpic and entropic contributions to the overall free energy of the binding reaction can also be determined in an ITC experiment.

The ITC instrument consists of two cells, one reference cell that contains water or a reference liquid, and one sample cell that contains one of the reactants, often the protein or macromolecule. These two cells are kept at a constant temperature in the system. The other reactant, is added to the sample cell through an automated syringe in small stepwise injections. Addition of ligand into the protein solution causes either release or consumption of energy, and this will either heat or cool the solution compared to the

reference cell. The ITC instrument will register the heat difference between the reference cell and the sample cell, and compensates by keeping the two cells at the same temperature (Wilson & Walker, 2010). The amount of power over time that is spent before the sample cell reaches its steady-state temperature after an injection of ligand is measured and is the experimentally determined quantity. This, so called corrected heat rate, is directly proportional to the heat of the reaction in the sample cell (Freire et al., 1990), and is given by equation 3.3

$$q = V\Delta H\Delta[L_b] \qquad \text{Equation 3.3}$$

Where q is the heat, V is the reaction volume, ΔH is the enthalpy of binding and $\Delta[L_b]$ is the change in bound ligand concentration.

The concentration of ligand in the syringe is often several fold higher than that of the protein in the sample cell, and after some injections, the proteins' binding sites become saturated. This effect can be observed from the recorded raw data as the peaks of applied power decreases because of the smaller change in heat for the reaction. Subsequent injections produce small peaks that correspond to dilution or mechanical effects which must be subtracted from the injection peaks before analysis (Leavitt and Freire, 2001). The raw data is fitted to a binding model which estimates the variable model parameters through equation 3.3. Analysis of the data yields the enthalpy (ΔH) and the association constant, K_a, of the interaction. These two parameters can further be used to calculate the Gibbs free energy (ΔG) and the entropy(ΔS) of the interaction. The most widely used model for the analysis of binding data is the Multiple Sets of Independent Binding Sites model, which assumes that all possible binding sites in the protein have the same affinity for the ligand. This model can be used for simple 1:1 binding. (Freire et al., 1990).

Execution

His- tagged Brd4 bromodomains were purified as described above (Section 3.2.3), and dialyzed to appropriate buffers. His-BD1 was dialyzed in Slide-A-Lyzer MINI units (MWCO 3,500) for 1h at 4 °C, to T7.5 buffer. His-BD2 was dialyzed overnight in Slide-A-lyzer cassettes (MWCO 3,500) to buffer T8.5. The difference in buffers was due to the different isoelectric points of the two domains (Table 3.5). After dialysis, the proteins were diluted to a concentration of approximately 40 μM in T7.5 or T8.5 buffer. Histone peptides were

prepared by weighing out the appropriate amount of lyophilized peptide, and dissolving it in either T7.5 or T8 .5 buffer to a concentration of approximately 1 mM. Peptide and protein concentrations were accurately measured by spectrophotometry NanoDrop, using extinction coefficients calculated with ProtParam (Table 2.13). Binding assays were performed at 25 °C with 20 continuous titrations of 2.03 µl 700- 1000 µM peptide into 300 µl 40 µM protein, with a constant stir rate of 300 rpm. Peptide titrated into buffer was used as a control/blank experiment, and was subtracted from collected data before applying a Multiple Sets of Independent Binding Sites model, which can be used for 1:1 binding.

4. Results

Acetylation of lysine 27 in histone H3 (H3K27ac) is a histone modification found in active enhancers, but not in primed or poised enhancers. Recognition of this mark by a specific reader protein might be important for enhancer activity and subsequent transcriptional activation at promoters. Brd4 was chosen as a candidate protein for specific recognition of H3K27ac due to its reported co-localization with this mark across the genome (Lovén et al., 2013), and previous large-scale bromodomain binding arrays which suggested interactions between the two (Filippakopoulos et al. 2012). To determine if Brd4 binds H3K27ac *in vitro*, and to characterize specificity and affinity of this interaction, binding assays with histone peptide binding pulldowns, isothermal titration calorimetry (ITC) and surface plasmon resonance (SPR) were performed. With these three methods, the interactions between bromodomains of Brd4 and synthetic histone tail peptides were studied. While histone peptide binding assays can give qualitative information on binding specificity, ITC and SPR can give quantitative information about the interactions, based on thermodynamics and kinetics respectively. Only the results from histone peptide binding assays and ITC are presented here, as technical difficulties rendered the SPR data unsuitable for interpretation.

4.1 Construction of human Brd4 bromodomain expression vectors

Both bromodomains of human Brd4 were to be tested for binding to H3K27ac, and thus different domain constructs containing either one or both bromodomains were created. Primers for two different sets of Brd4 constructs were created, one set which included only the core bromodomain sequences with five flanking residues on either side (BD1-s and BD2-s), and one set where BET-family-specific flanking sequences were included (BD2 and BD2) (Figure 4.1 and 4.2). A construct containing both Brd4 bromodomains, BD1 and BD2, was also created (Figure 4.2), however, this construct was not used in further experiments as it exhibited severe degradation after purification. In addision, primers for the creation of a full-length Brd4 construct were also prepared, but PCR amplification of this sequence was unsuccessful. Human Brd4 bromodomain sequences were retrieved from UniProtKB (BRD4_HUMAN). As can be seen from the multiple sequence alignment in figure 4.1, Brd4 bromodomain sequences retrieved from UniProt (BD1-s and BD2-s) did not include all secondary structure elements. Brd4 constructs were

created by PCR of cDNA from HeLa cells, and subsequent cloning into pSXG (for expression of GST-fusion proteins) and pQE30 (for expression of His-tagged proteins) expression vectors. Pilot protein expressions of the Brd4 constructs showed higher protein expression levels from constructs that contained BET-specific flanking amino acids, and consequently these constructs were used for the expression of Brd4 bromodomains for later binding assays.

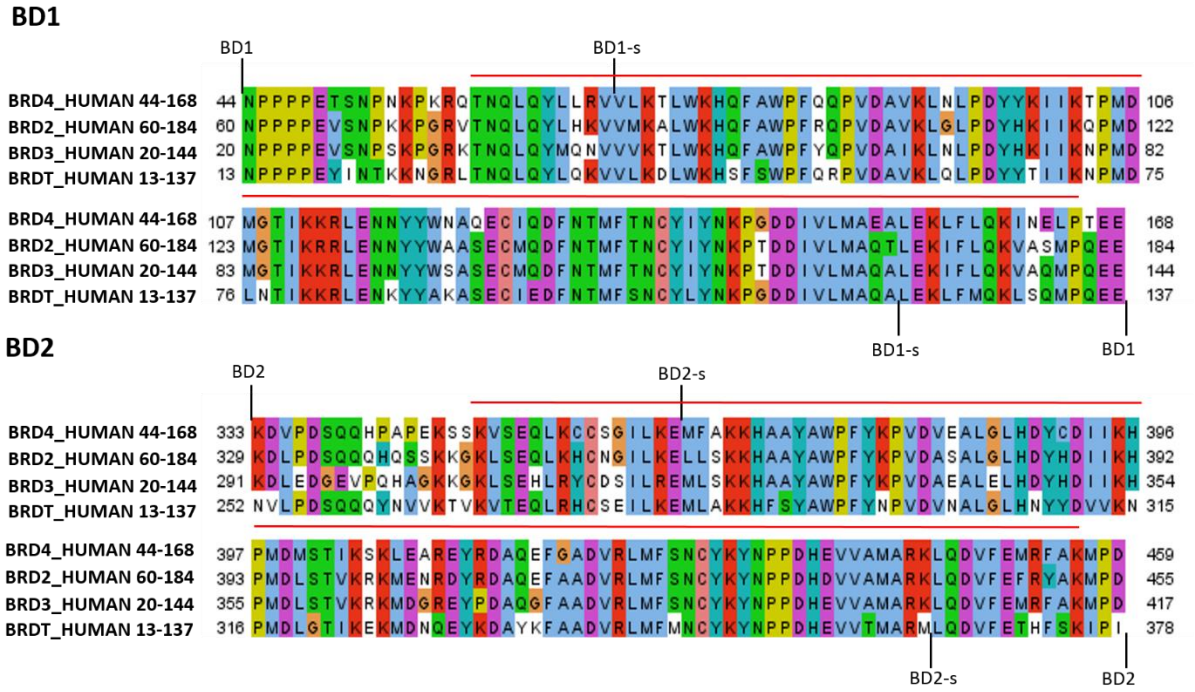

Figure 4.1: Multiple sequence alignments of BD1 and BD2 of the human BET-family: BD1 and BD2 marked by black lines, indicate Brd4 BD1 and BD2 bromodomains with BET-family specific flanking sequences. BD1-s and BD2-s: shorter constructs that were made from BD1 and BD2 sequences retrieved from UniProtKB. BD1 and BD2 secondary structure are indicated with red lines, and was found from BD1 (2OSS) and BD2 (2OUO) crystal structures in PDB. Multiple sequence alignments were created with Clustal Omega.

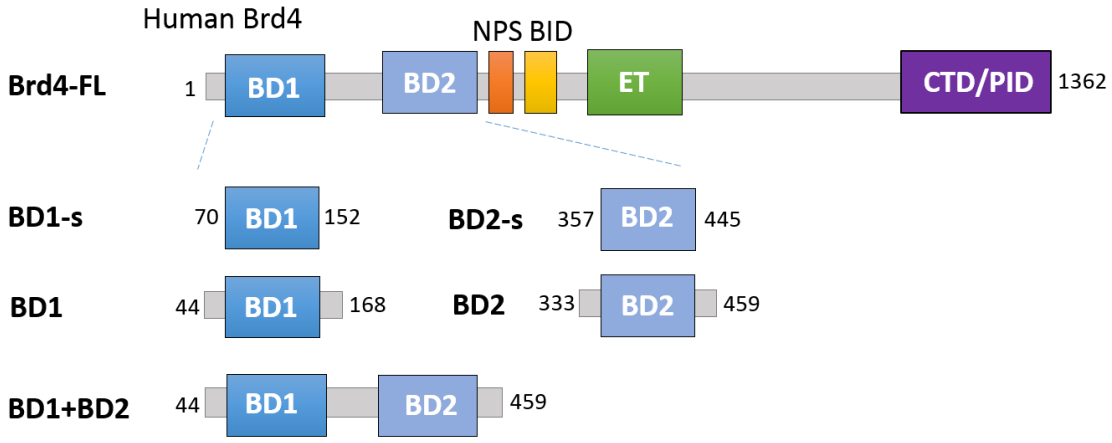

Figure 4.2: Brd4 bromodomain constructs. Brd4-FL: Construct containing the entire Brd4 sequence. BD1, BD2 and BD2+BD2: Brd4 bromodomain constructs containing BET-family specific flanking sequences. BD1-s and BD2-s: Shorter Brd4 bromodomain constructs containing only the core bromodomain sequence, as found in UniProtKB.

4.2 Expression and purification of GST-bromodomain fusion proteins

GST- Brd4 bromodomain proteins, expressed from the pSXG vector, were used in histone peptide binding assays. In addition to enhancing protein stability and solubility (Nygren et al., 1994), the GST-tag enabled immunoblotting of fusion proteins, as there are no available antibodies for specific recognition of the Brd4 bromodomains. GST-bromodomain fusion proteins were bacterially expressed in *E.coli* BL21-RIL at 18˚C over-night, (Section 3.21). The GST-fusion bromodomain from human acetyl-transferase p300 (HUMAN_EP300), denoted p300B, and GST alone were also expressed to serve as positive and negative controls in the following experiments.

GST-fusion bromodomains were found to be soluble and exhibited low levels of degradation after expression, indicated by the presence of a polypeptide migrating as 25 kDa, corresponding to the GST part of the fusion proteins (Figure 4.3). The bacterially expressed proteins were purified by GST-affinity chromatography (Section 3.2.2). As the vast majority of proteins in the eluate fraction had the expected molecular sizes (Figure 4.4), the affinity-purified proteins were used directly for histone peptide binding assays.

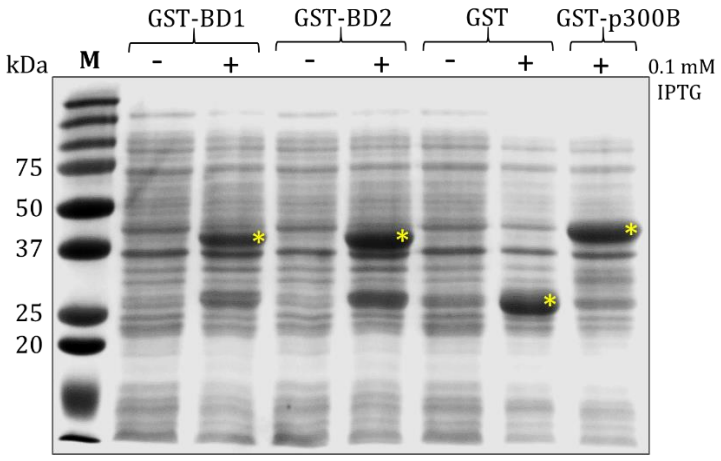

Figure 4.3: Expression of GST-fusion Brd4 bromodomains BD1 and BD2, and control proteins. Protein expression was induced with 0.1 mM IPTG at 18˚C over-night, and verified by SDS-PAGE analysis followed by Coomassie staining. 10 µl whole cell lysate was loaded. Bands of interest are indicated with yellow asterisks, and have the following expected molecular weights: GST-BD1; 42.3 kDa, GST- BD2; 42 kDa, GST; 25.7 kDa and GST-p300B; 41.3 kDa.

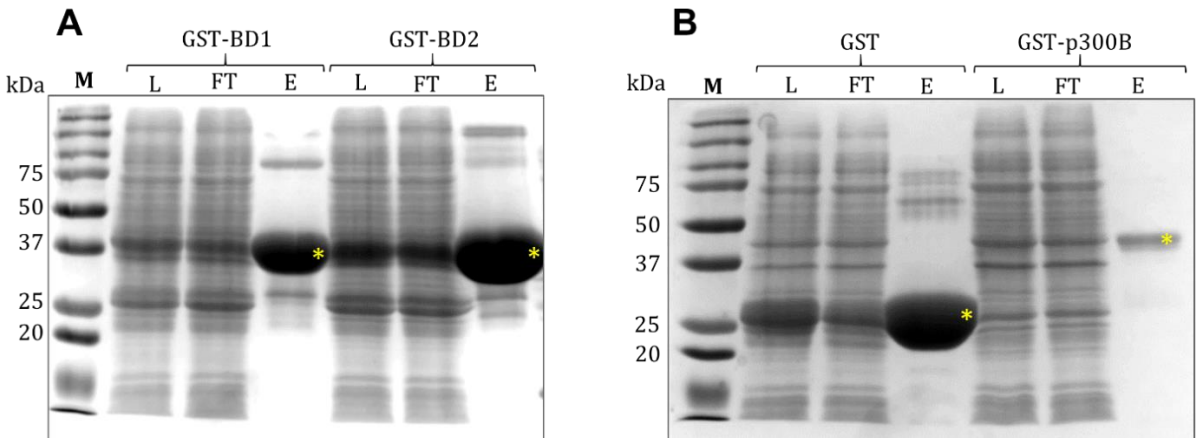

Figure 4.4: Purification of Brd4 bromodomains by GST-affinity chromatography. 5 µl of each fraction was analyzed by SDS-PAGE followed by Coomassie staining. Purified proteins of interest are marked by yellow asterisks. (**A**): GST-BD1 (42.3 kDa) and GST-BD2 (42 kDa). **(B):** p300B (41.3 kDa) and GST (25.7 kDa). L: whole bacterial lysate, FT: resin flow-through, E: eluate

4.3 Histone peptide binding assays show no interaction between Brd4 bromodomains and H3K27ac

The first binding study performed to test the potential binding between Brd4 bromodomains and H3K27ac was a histone peptide binding assay. The assay was performed with GST-fused Brd4 bromodomains and a panel of synthetic biotinylated histone peptides. The biotin moiety on the peptides allowed the separation of GST-fusion proteins bound to histone peptides from unbound protein, through the precipitation of peptide-protein complexes with streptavidin-coated Sepharose beads. The GST moiety served as an epitope tag in the subsequent analysis of the complexes by SDS-PAGE immunoblotting. Non-modified (H3 and H4) and methylated (H3K27me1) histone peptides were included as negative controls, while a H4 peptide acetylated at K5, K8, K12 and K16 (H4tetra-ac) was included in the experiments as a positive control for bromodomain binding. Many bromodomains, including BD1 and BD2 of Brd4, have been reported to have higher affinities for peptides that have two acetyl-lysines separated by 1-5 amino acids (Morinière et al., 2009). An H3 histone peptide acetylated at both K27 and K23 (H3K23,K27ac) was therefore included in the assay to determine if the additional acetyl-lysine would be a better ligand for BD1 and BD2. The bromodomain of acetyltransferase p300 is known to bind H4tetra-ac histone peptides (Rack et al., 2014) and was therefore used as a positive control in the peptide pulldown assay, while GST

alone was included as a negative control. To check the possibility of unspecific binding of the proteins to the streptavidin- conjugated beads, an experiment without histone peptides was also performed. Different peptide to protein molar ratios were tested for histone peptide binding assays, and a ratio of 10:1 (1:0.1 μM) peptide to protein was found to be most suitable as it gave the lowest level of unspecific binding.

Four replicates of peptide binding assays were performed with each fusion protein. In all experiments GST showed a low level of binding to all biotinylated peptides, whereas GST-p300B and GST-BD1 showed strong binding to H4tetra-ac peptide (Figure 4.5). GST-BD2 binding to H4tetra-ac peptide was detected in only one experiment (Figure 4.4.B). A low level of unspecific binding to the beads was detected, especially in the case of GST-BD1 (Figure 4.4.A). The rather strong signal was present only in one out of three replicates that included a "beads only" control. Compared to background signals, no binding of the fusion proteins to modified H3 peptides, including H3K27ac, was detected.

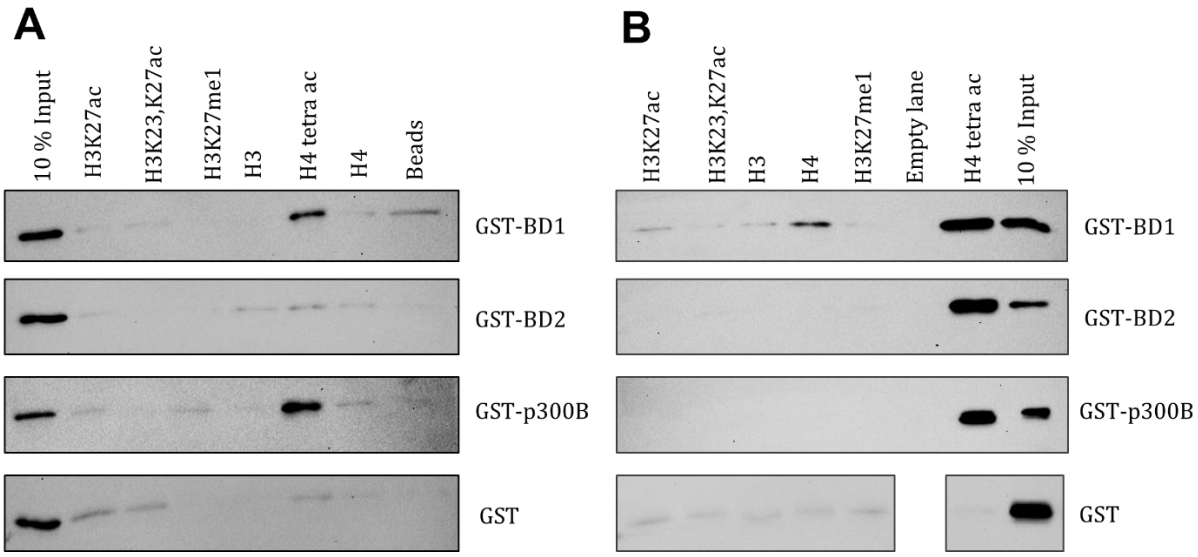

Figure 4.5: Histone peptide binding assays show no specific binding between Brd4 bromodomains and H3K27ac peptide. Biotinylated histone peptides and recombinant GST-BD1, GST-BD2, GST-p300B and GST were used as indicated. 10% of input and 33% of eluate fractions were analyzed after SDS-PAGE by immunoblots using anti- GST antibody. Abbreviations: H3/H4, non-modified histone peptides (residues 1-21 aa and 2-24 aa, respectively.) H4tetra-ac: H4 peptide acetylated at K5,8,12, and16. Two replicates of four experiments are presented in A and B.

4.4 Expression and purification of His-tagged Brd4 bromodomain proteins

As our peptide binding assays gave conflicting results compared to previously published studies (Filippakopoulos et al., 2012), ITC was employed for determining whether Brd4 bromodomains bind to the H3K27ac peptide. As the presence of the GST-moiety could disturb measurements in ITC, His-tagged Brd4 bromodomain constructs were created. The same Brd4 bromodomain sequences as for GST-constructs were used for the His-tagged constructs (Figure 4.1). Protein expression was carried out in *E.coli* M15 cells over-night at 18 ˚C, and analyzed with SDS-PAGE and subsequent Coomassie staining (Figure 4.6). Samples from induced bacterial cultures showed high level of expression of all Brd4 bromodomain constructs.

Expressed His-tagged Brd4 bromodomain proteins were purified using immobilized metal affinity chromatography (IMAC) (Figure 4.7). His-BD1+BD2 protein exhibited a severe degradation pattern after purification (data not shown), hence this construct was not used in following experiments. His-BD2 had a high purity, as bands not corresponding to the expected protein size were very weak after Coomassie staining. A more intense band of lower molecular weight was visible in the eluate lane of His-BD1. A band of this size can be seen in the lysate of both His-BD1 and His-BD2, but it is only retained in the eluate of His-BD1 (Figure 4.7). Using Bio-Rad's Image Lab software to determine the relative intensity of the bands, purified His-BD1 gave an estimated purity of 85-90%. His-BD1 was, however, not stable in solution, and started to precipitate 3 hours after purifications. Precipitation of His-BD2 was observed two days after purification, when stored at 4˚C.

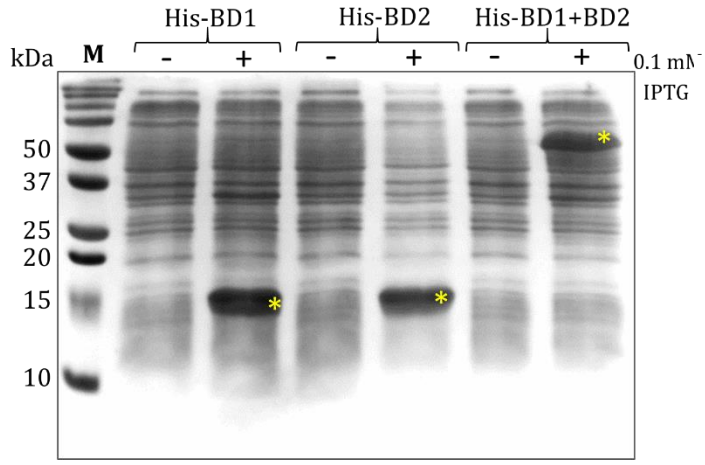

Figure 4.6: Expression of His-tagged Brd4 bromodomains BD1 and BD2. Protein expression was induced with 0.1 mM IPTG at 18˚C over-night, and verified by SDS-PAGE analysis followed by Coomassie staining. 10 µl of whole cell lysate was loaded. Bands of interest are indicated with yellow asterisks, and have the following expected molecular weights: His-BD1:16.3 kDa, His- BD2: 16 kDa. His-B1+BD2: 48.3 kDa.

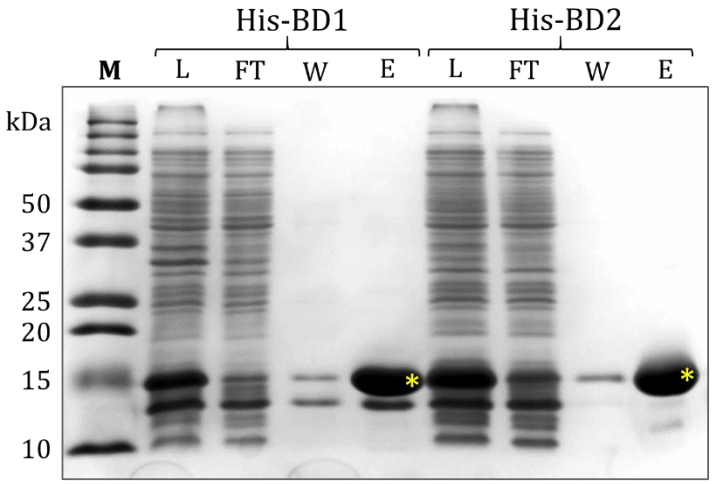

Figure 4.7: IMAC purification of His-tagged Brd4 bromodomains. His-tagged proteins were purified on a Ni-NTA agarose IMAC column. 5 µl of each fraction was analyzed by SDS-PAGE followed by Coomassie staining. Purified proteins of interest are marked by yellow asterisks: His-BD1 (16.3 kDa), His-BD2 (16.0 kDa). L: whole bacterial lysate, FT: column flow-through, W: column wash E: eluate.

4.5 Analysis of His-tagged bromodomain aggregation by SEC and DLS

As His-BD1 showed signs of precipitation after purification, measurements of particle sizes and degree of aggregation were performed by size exclusion chromatography (SEC) and dynamic light scattering (DLS). His-BD1 precipitated in several tested buffers, including Tris and HEPES buffers at pH 6.7, 7.5, 8.5 and 9. There was a slight decrease in the extent of precipitation of His-BD1 in buffers with 50 mM Tris and 300 mM NaCl compared to buffers with 50 mM Tris and 150 mM NaCl. After overnight storage at 4˚C

there were however visible signs of precipitation even in buffers with higher salt concentration.

4.5.1 His-BD1 aggregates in solution

SEC was performed to investigate if purified His-BD1 was present as a monomer, or in higher oligomeric states. The molecular weight of species present in the His-BD1 elution profile were estimated from a standard curve made from a selection of calibration proteins of known molecular weight. The calibration proteins were separated by SEC in the same manner as His-BD1 (Figure 4.8.B), and a standard curve was made by plotting the partition coefficient, K_{av}, calculated from their elution points (Equation 3.2), as a function of the logarithm of their molecular weights. Linear regression of this plot yielded equation 4.1, which was subsequently used to calculate the molecular weights of proteins in the His-BD1 sample. The calculated values are however indicative, as there is no perfect correlation between stokes radius and molecular weight, as the proteins can have different shapes

The elution profile of His-BD1 displayed three distinct peaks (**b**, **c** and **d**) indicating that the sample contained particles of three different sizes (Figure 4.8.A). An additional signal not present in the calibration standards was detected in the void volume of His-BD1 (**a**). The molecular weight of particles eluted in the void volume cannot be determined from a calibration standard curve, as their sizes are too large. Only two different proteins can be identified from SDS-PAGE of His-BD1 prior to SEC (Figure 4.7), one intense band corresponding to His-BD1, and a weaker, smaller band that might be an impurity or a degradation product.

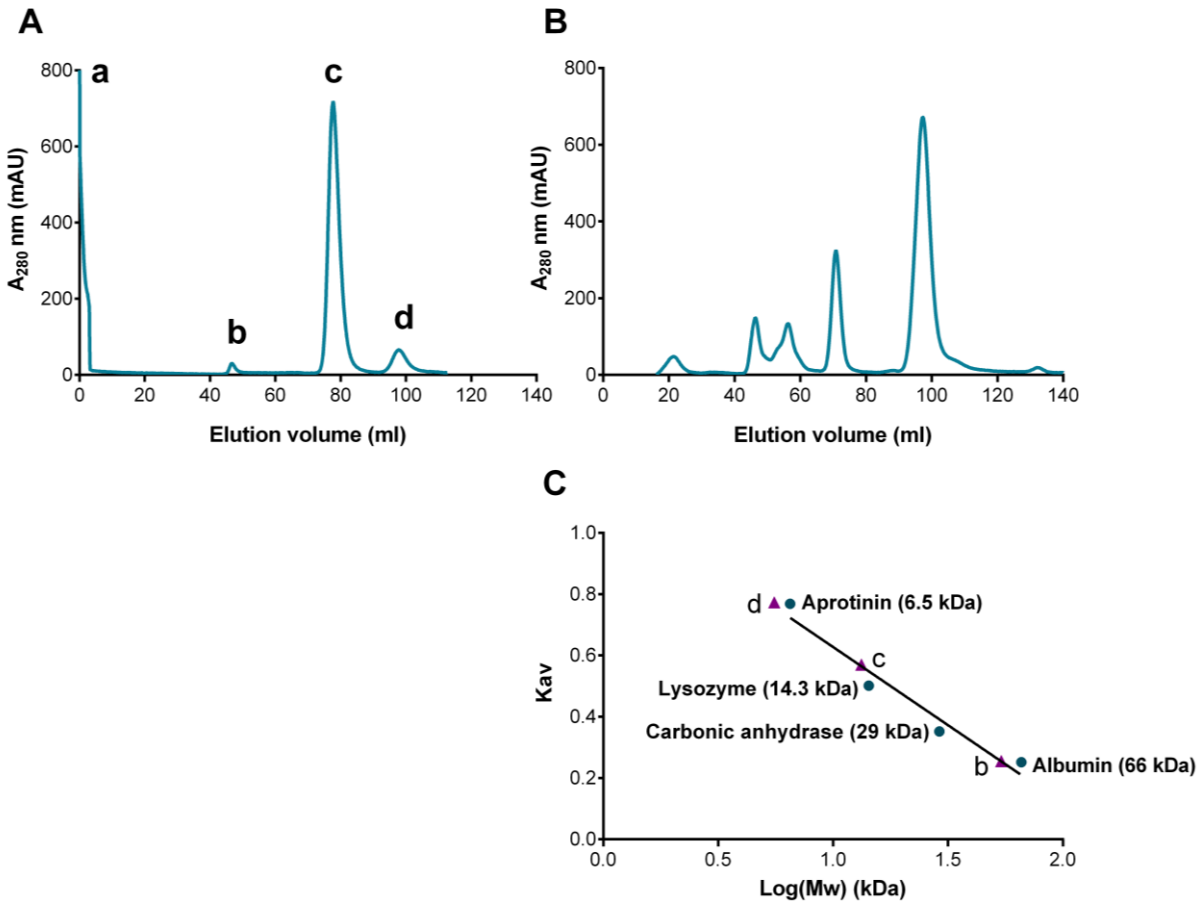

Figure 4.8: SEC elution profile of his-BD1 and standard proteins. Separation by SEC was performed in a 120 ml Superdex 16/600 column, at flow rate 1 ml/min. **A:** Elution profile of His-BD1. A 0.5 ml sample of 245 µM His-BD1 was loaded on the column. **B:** Elution profile of a series of standard proteins; Albumin (66 kDa), Carbonic anhydrase (29 kDa), Lysozyme (14.3 kDa) and Aprotinin (6.5 kDa). Blue dextran (~2,000 kDa) was included to estimate the void volume V_o. **C:** SEC calibration curve of the partition coefficient K_{av} of selected protein standards as a function of their log molecular weight (kDa). Peaks from SEC of His-BD1 (**A**) are shown as triangles. R^2 of regression was 0.95.

$$K_{av} = -0.51Mw + 1.14$$

$$Mw = \frac{K_{av} - 1.14}{-0.51}$$

Equation 4.1

A molecular weight of 13 kDa was calculated for peak **c** in His-BD1. The theoretical molecular weight of His-BD1 is 16.3 kDa, and therefore this peak was assumed to correlate with monomeric His-BD1. Since the area under peak **a,** which was eluted in the void volume, could not be determined, it was not possible to calculate the fraction of monomeric His-BD1 in the sample. Peaks **b** and **d**, the two smaller peaks observed in the

elution profile, were estimated to be 53 and 5 kDa, respectively. No polypeptide migrating as 53 kDa is visible in SDS-PAAG of His-BD1, which suggests that the presence of this peak in the SEC data is due to aggregation of His-BD1 into a larger complex. The molecular weight of the species eluted in the void volume (peak **a**) could not be determined, but its presence also suggests that His-BD1 forms large aggregates in solution.

4.5.2 DLS of His-BD1 revealed extensive aggregation

As SEC experiments suggested that His-BD1 aggregated in solution, dynamic light scattering (DLS) was performed to investigate the particle size distribution of His-BD1. The hydrodynamic particle sizes of His-BD1 were measured after 20 minutes centrifugation to remove insoluble particles. The monomeric protein lysozyme (14.3 kDa) was included as a control, as it has similar molecular weight as His-BD1 (16.3 kDa). Three independent particle-size readings were made for each protein. The particle size measured by DLS is called hydrodynamic diameter, and gives the diameter of a hard sphere that migrates like the measured particle in solution. However, in practice, particles and macromolecules in solution are non-spherical and surrounded by a hydration shell. Because of this, the reported particle diameter will give an indication of the apparent size of the dynamic solvated particle. The hydrodynamic particle sizes determined by these DLS experiments are not considered to give the absolute size of the molecules, but to give indications of the oligomeric state of the proteins in question. The DLS data presented here are the first order results from the experiments, where an intensity distribution of particle sizes is shown. The particle scattering intensity is proportional to the square of the molecular weight, and therefore this distribution is a sensitive detector for the presence of large particles and aggregation. This means that more weight is given to larger particles in the intensity distribution, and that the reported intensity peaks are not proportional to the number of particles with each diameter.

For His-BD1, five peaks were observed from the DLS data (Figure 4.9.A). Peaks 3 and 5 were only found in the first and third reading, while 2 and 4 were only observed in the second reading. The peak with the highest intensity present in His-BD1 had a mean hydrodynamic diameter of 6.2 nm, and a peak diameter of 5.6 nm. The particle size

measurement of lysozyme revealed only one peak, as expected (Figure 4.9.B). The collected data from DLS measurements of His-BD1 and lysozyme are summarized in table 4.1.

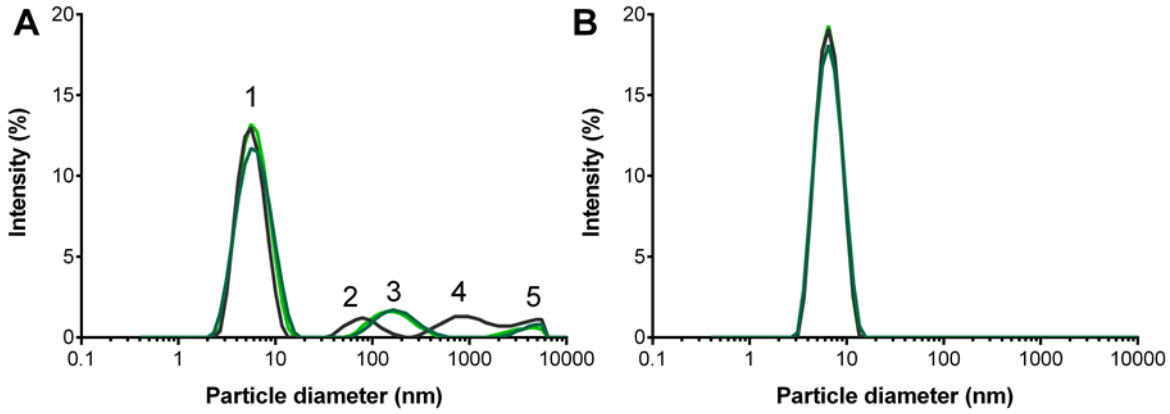

Figure 4.9: The His-BD1 sample is polydisperse: Particle sizes were measured by DLS. **A:** Three independent readings of the particle size distribution of a His-BD1 sample (214 µM). Three separate readings are shown in different colors. **B:** Three independent DLS readings of the particle size distribution of lysozyme (300 µM).

Table 4.1: Particle size distribution of His-BD1 and lysozyme

Peak	Mean particle diameter* (nm)	Intensity (%)	Peak Area intensity (%)	Calculated÷ Mw (kDa)
1	6.4[1], 5.8[2], 6.2[3]	11.7, 13.0, 13.2	83.0, 73.5, 82.7	52.3, 40.5, 48.1
2	84.8[2]	1.2	7.5	41,180
3	192[1], 175[3]	1.7, 1.6	13.5, 13.6	350,655; 275,786
4	1054[2]	1.3	12.9	Too large
5	4285[1], 3756[3]	0.8, 0.6	3.5, 3.6	Too large
Lysozyme	5	19.1	100	27.5

*Two times stokes radius
[1,2,3] Readings 1,2 and 3
÷ $r = 0.483(Mw)^{0.386}$ – r: Stokes radius (Å), Mw: Molecular weight (kDa) (Venturoli and Rippe, 2005)

SDS-PAGE of His-BD1 showed two proteins present after purification, one corresponding to the expected size of His-BD1, and a smaller, less abundant protein. However, there is no indication of the presence of a smaller particle with low intensity in the DLS results. Peaks 2,3,4, and 5 indicate the presence of large aggregates in the sample. The width of the particle size distribution is reported as dimensionless parameters known as the polydispersity index (Pdi). This value describes the degree polydispersity in a sample. Values smaller than 0.05 are rare, and most often seen only in highly monodisperse standards, while a Pdi greater than 0.7 indicates a very broad size distribution which is not suitable for DLS (Malvern Instruments 2011). Samples with a Pdi below 0.1 are usually considered monodisperse. The Pdi of His-BD1 was reported as 0.3, while that of lysosome was found to be 0.06. These data indicate that His-BD1 aggregates in solution, and causes the formation particles of larger and varied sizes.

4.5.3 His-BD1 exhibits rapid aggregation

To determine the rate and extent of the aggregation, an experiment was performed where the particle sizes of His-BD1 were recorded every 5 minutes for a time period of approximately 16 hours. The collected data points were examined and the intensity of peaks that formed or declined over the time course were plotted (Figure 4.10). Only particles that showed a stable presence in the sample were plotted, and peaks that rapidly formed and declined are not shown. The plotted particles were followed by their peak diameter, and not the mean diameter calculated from the width of their curves. Three peaks were found to stably inhabit the His-BD1 sample, corresponding to peaks 1,3 and 4 from figure 4.9.A. The plot of His-BD1 particle distribution over time showed a decrease in intensity of peak 1, assumed to be the monomeric form of His-BD1, over time. After only 56 minutes, the intensity of peak 1 was halved. The intensity of peak 3, however, increased by 4 times in the same time period.

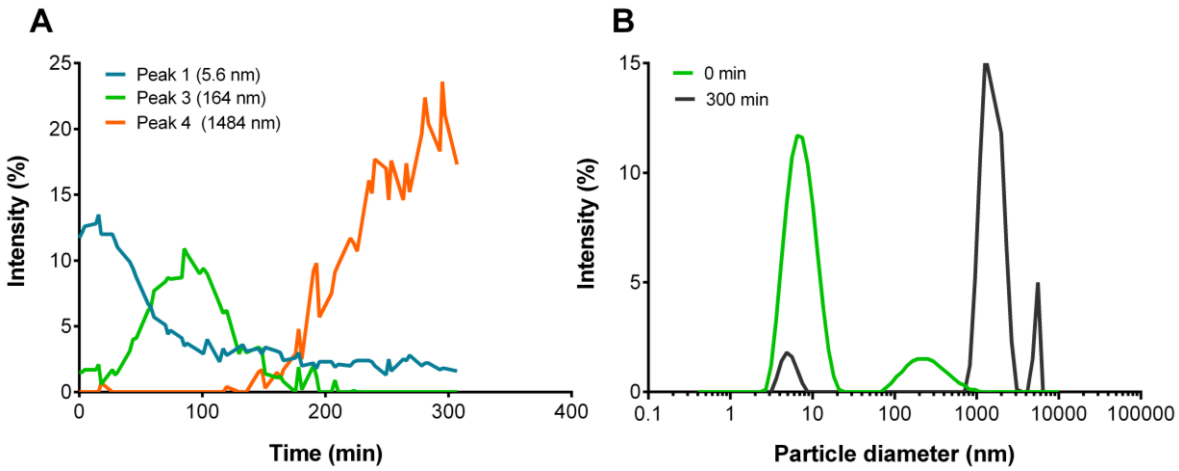

Figure 4.10: His-BD1 aggregation over time: Particle sizes were measured by DLS. **A:** The particle size distribution of a His-BD1 sample (245 µM) was monitored over time by 5 minute interval readings over a time course of 16 hours. Only the first 300 minutes are presented. **B:** The particle size distribution of the His-BD1 sample (245 µM) at the start of the experiment, 0 min, and after 300 minutes.

After 300 minutes, the sample was dominated by peak 4, a large particle with a diameter of 1484 nm. The intensity of peak 1 never reached zero, but stayed at a constant level of 2-3% after the first 100 minutes. After the 300 minutes shown in figure 4.10.A, the data became uneven and large spikes in intensities were observed. The spikes in intensity obscured the data, and therefore only the first 300 minutes of the time-scale are presented. The particle size distribution of His-BD1 after 300 minutes was drastically different from that seen at the start of the experiment (Figure 4.10.B). As large particles obscure the presence of smaller ones, the fraction of monomeric His-BD1 after 300 minutes is not known. The polydispersity index also changed over time. At the start of the experiments it was 0.29, but after 300 min, it was 0.43. The polydispersity was at its highest after 150 minutes, with a value of 1. It is important to note that in polydisperse samples, which have a polydispersity index above 0.1, the reported particle sizes have large deviations. These data suggest that His-BD1 aggregated rapidly over time, and that after 300 minutes, a large aggregate with a diameter exceeding 1000 nm was formed.

4.5.4 DLS also revealed aggregation of His-BD2

His-BD2 showed no visible signs of aggregation in the form of precipitation after purification, but particle size measurements with DLS showed that His-BD2 was not present as an entirely monomeric protein. Three distinct peaks which correlate with the

presence of three particle sizes were seen from DLS data of His-BD2 (Figure 4.11). The peak of the highest intensity was found to have a mean hydrodynamic particle diameter of 6.4 nm (Peak 1), while the second prominent peak indicates the presence of a larger particle with a mean diameter of approximately 100 nm (Peak 2). Furthermore, a wide peak is also present at around 1100 nm (Peak 3). The Pdi of the sample was 0.5. The estimated molecular weights of the peaks and a summary of the His-BD2 size distribution measurements is presented in table 4.2. The His-BD2 sample that was used for DLS measurements was not centrifuged before measurements were performed. This can explain the apparent higher intensity of the larger 100 nm peak compared to His-BD1 which displayed stronger visual signs of aggregation. No time-course experiments were performed with His-BD2. The collected data suggested that there was some degree of aggregation into larger complexes in the case of His-BD2 as well. Due of the rapid aggregation observed with DLS, His-BD1 and His-BD2 samples were freshly purified immediately before ITC and SPR experiments, and kept at low concentrations.

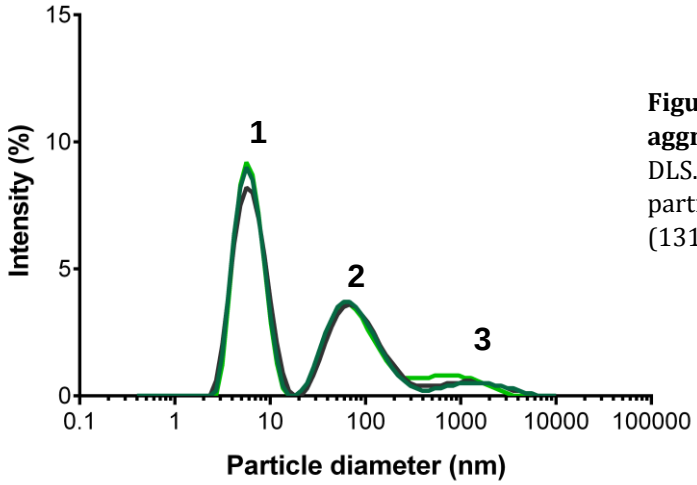

Figure 4.11: His-BD2 shows signs aggregation. Particle sizes were measured by DLS. Three independent readings of the particle size distribution of a His-BD2 sample (131 µM) are shown in different colors.

Table 4.2: Particle size distribution of His-BD2

Peak	Mean particle diameter* (nm)	Intensity (%)	Peak Area intensity (%)	Calculated÷ Mw (kDa)
1	6.4	9.0	54.7	52.3
2	96.3	3.7	37.7	78,866
3	1136	0.5	7.6	Too large

*Two times stokes radius

÷ $r = 0.483(Mw)^{0.386}$ – r: Stokes radius (Å), Mw: Molecular weight (kDa) (Venturoli and Rippe, 2005)

4.6 ITC with Brd4 bromodomains

To validate the results acquired from histone peptide binding assays, which showed no binding between Brd4 bromodomains and H3K27ac, ITC measurements were performed. ITC was carried out with His-tagged Brd4 bromodomains and H3K27ac/H4tetra-ac peptides. Measurements with H4tetra-ac were included as a positive control.

4.6.1 Brd4 BD1 shows no apparent binding to H3K27ac

ITC experiments were performed with His-tagged BD1 purified by IMAC (Section 3.2.3). Since extensive and rapid aggregation was observed for His-BD1, ITC measurements were carried out directly after purification and dialysis, and the samples were centrifuged for 20 minutes before use. Three independent experiments for His-BD1 binding to H4tetra-ac were performed, but only two experiments were conducted for determining the binding to H3K27ac, as they showed negative results. ITC with His-BD1 and H4tetra-ac showed a typical pattern for binding reactions (Figure 4.12.A). Each peak represents one injection. The heat of dilution was measured in a separate experiment, by titrating H4tetra-ac into T7.5 buffer. The collected ITC data was fitted to a model for 1:1 binding (Figure 4.12.B). Models fitted to ITC data exhibiting binding are expected to have a sigmoidal shape. This was not the case for ITC experiments with His-BD1 and H4tetra-ac, as they lacked the lower plateau. The standard deviations of collected data points were large, which is most likely due to the instability of baseline which was observed for all ITC measurements with His-BD1 (Figure 4.12), and experiments done at longer intervals from purification had increasingly more unstable baselines, even after centrifugation of the proteins. Titrations of H4tetra-ac peptide in T7.5 and T8.5 buffer, however, showed a stable baseline with even peaks (Figure 4.12.B). Due to this, parameters calculated from the fitted model should be interpreted with care.

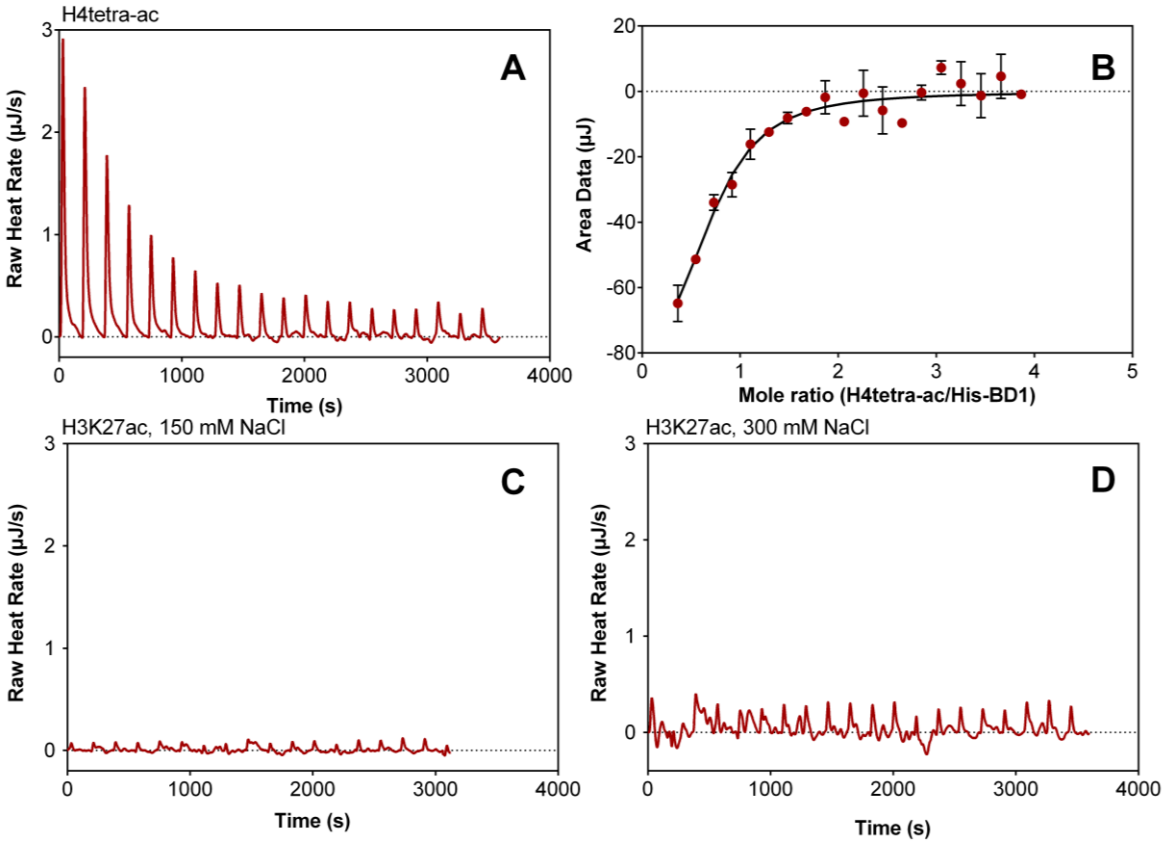

Figure 4.12: ITC of his-BD1 with H4tetAc and H3K27ac. ITC measurements were performed in a ITC Nano instrument from 20 titrations of 2.03 µl were introduced into the sample cell containing 300 µl His-BD1. **A:** 1.01 mM H4tetra-ac peptide titrated into 40 µM his-BD1. Each peak represents with one titration. **B:** Total heat of injection (µJ) of data shown in **A**, plotted as the area data of raw heat rate (µJ/s) against the mole ratio of H4tetra-ac to His-BD1. The error bars show the standard deviation between triplicates. The first data point has been removed, as it tends to give a low heat signal due to diffusion from the syringe as the system equilibrates before the first injection. The data have been fitted to a model assuming independent binding sites. **C:** 0.79 mM H3K27ac peptide titrated into 40 µM His-BD1, 150 mM NaCl **D:** 0.78 mM H3K27ac peptide titrated into 40 µM His-BD1, 300 mM NaCl.

A dissociation constant (K_D) of 5.3 µM ± 0.33 and an n- value of 0.66 ± 0.11 were determined from the model of binding between His-BD1 and H4tetra-ac peptide. The n-value gives the stoichiometry of the binding reaction, where a value of 1 indicates a 1:1 binding.

No typical binding pattern was observed in ITC experiments with His-BD1 and H3K27ac (Figure 4.12.C). The recorded heat rates are low, and equal the heat of dilution. No apparent binding between His-BD1 and H3K27ac can be seen from the curve. In experiments with H3K27ac a lower concentration of peptide was utilized. An initial experiment was done with 200 µM peptide and 20 µM protein, but this yielded low heat signals and the concentrations were raised to 0.79 mM H3K27ac peptide and 40 µM His-BD1. After experiments with higher concentrations still gave no signals that indicated

binding, it was deemed unnecessary to increase the concentrations further. An additional ITC experiment was performed with H3K27ac and His-BD1, with 300 mM NaCl rather than 150 mM NaCl (Figure 4.12.D). Earlier observations of the precipitation of His-BD1 indicated that the domain possibly precipitated at a slower rate in a 300 mM NaCl buffer. However, no binding between His-BD1 and H3K27ac was observed under high salt conditions either, and the stability of the baseline was not increased. Interestingly, the baseline seemed to be more disturbed with a 300 mM buffer than with a 150 mM, and the heat rates were bigger. ITC experiments showed that His-BD1 binds H4tetra-ac, but not H3k27ac.

4.6.2 His-BD2 shows no apparent binding to H3K27ac

ITC experiments with His-BD2 were carried out in the exact same manner as for His-BD1, but a buffer with pH 8.5 was used due to its different pI value (Table 3.5). The ITC data of His-BD2 and H4tetra-ac showed a decrease in heat rate during H4tetra-ac titration, from 0.6 µJ/s to around 0.2 µJ/s (Figure 4.13.A). Titrations of the same concentration of H4tetra-ac into T8.5 buffer showed the heat of H4tetra-ac dilution to be about 0.2 µJ/s per injection (Figure 4.13.B). This could indicate that there was some interaction occurring between H4tetra-ac and His-BD2, and as further injections of peptide were made, the system saturated. However, the injection peaks were uneven, and the baseline was disturbed which precluded fitting a model to the data. As depicted in the figure, some peaks have small bumps, which could be caused by heat being generated through domain-domain interactions. These “bumps” increase the area under the peak, which causes the integrated data used for model-fitting to become inaccurate. Because of this, and the unevenness of the peaks themselves, the calculated area data does not form a sigmoidal pattern that could be modeled. The heat rates are also very low, making it harder to distinguish them from the baseline. Higher heat rates could be achieved by increasing peptide and protein concentrations further, but at 1 mM and 40 µM, the concentrations are already quite high. The ITC data of His-BD2 and H3K27ac showed no typical binding pattern, and a very disturbed baseline where the individual injections were hard to distinguish (Figure 4.13.C). No binding between His-BD2 and H3K27ac was indicated from the data. Table 4.3 summarizes the ITC results of His-tagged Brd4 BD1 and BD2 with H4tetra-ac and H3K27ac.

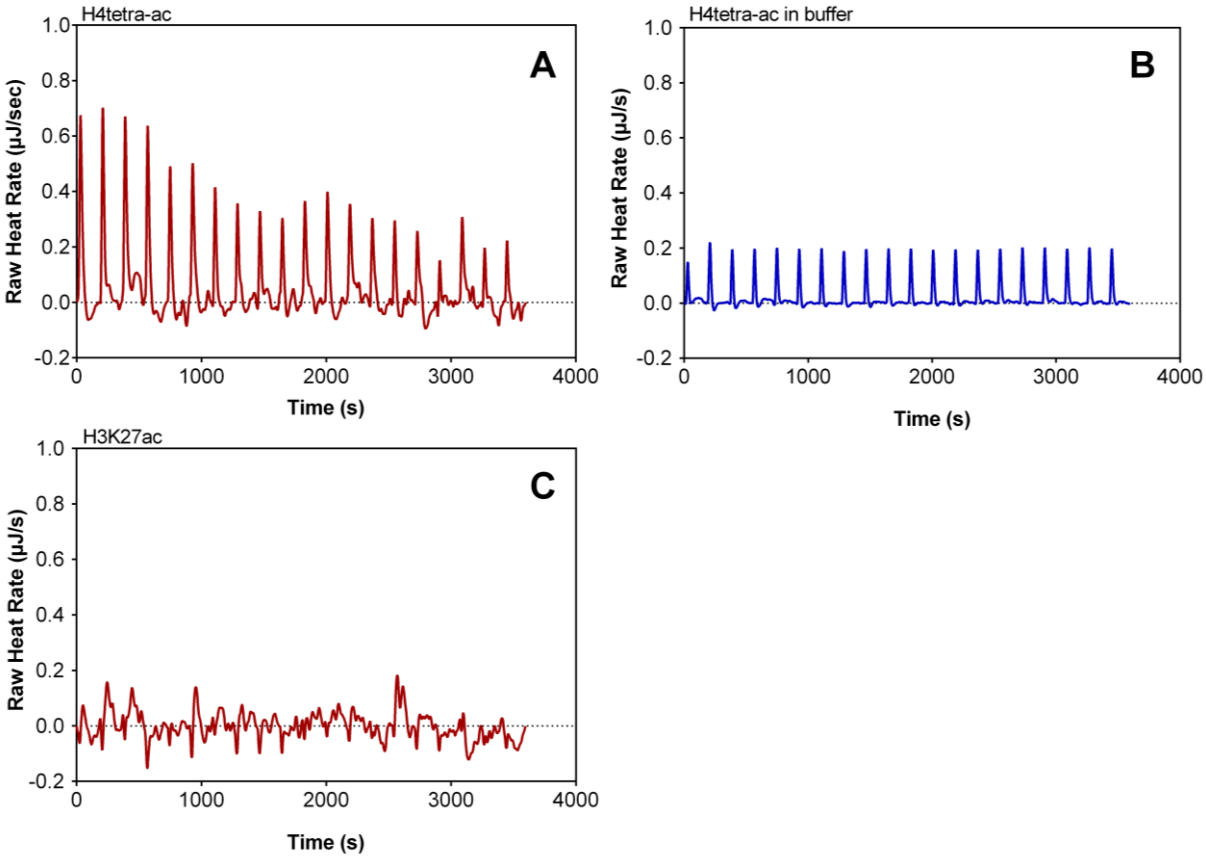

Figure 4.13: ITC of His-BD2 with H4tetAc and H3K27ac. 20 titrations of 2.03 µl were introduced into the sample cell containing 300 µl protein/buffer, with a stirring rate of 300 rpm. **A:** 1.03 mM H4tetra-ac peptide titrated into 43 µM His-BD2. Each peak represents one titration. **B:** 1.03 mM H4tetra-ac peptide titrated into T8.5 buffer. This shows the heat of dilution of H4tetra-ac in T8.5 buffer. **C:** 0.78 mM H3K27ac peptide titrated into 41 µM His-BD2. Note that the range of the y-axis does not correspond to figure 4.12.

Table 4.3: ITC of Brd4 bromodomains

Domain	Histone mark	Protein[1] (µM)	Peptide[2] (mM)	n-value[3]	K_d (µM)
His-BD1	H4Tetra ac	40	1.01	0.66 ± 0.11	5.3 ± 0.31
	H3K27ac	40	0.79	-	-
His-BD2	H4Tetra ac	43	1.03	-	-
	H3K27ac	41	0.78	-	-

[1]: Protein concentration in the sample cell before titration

[2]: Peptide concentration in the syringe before titration

[3]: The n-value gives the amount of binding sites per protein

5. Discussion

Differences between cell types arise from differences in their gene expression profiles. Enhancers are the major determinants differential gene expression and cell type specificity (Bulger and Groudine, 2010). They activate gene expression by bringing transcription factors and co-activators to the promoters they regulate. Genomic regulatory elements, like enhancers, have been shown to be enriched in specific combinations of histone PTMs, correlating to their state of activity. PTMs on histone tails can influence the regulation of genes through both disrupting nucleosome interactions and recruiting specific proteins that have roles in gene transcription (Ruthenburg et al., 2007). Active enhancers are enriched with an acetylation mark on lysine 27 of histone H3 (Creyghton et al., 2010). The role of this mark is not yet understood, but its enrichment at enhancers distinguishes active from primed and poised enhancers (Creyghton et al., 2010). Histone PTMs are recognized by specialized reader domains, which in turn are part of or recruit proteins with different effector functions. Hence, the aim of this work has been to find a reader protein that specifically recognizes H3K27ac.

In this project, Brd4, a bromodomain-containing protein previously shown to be involved in transcriptional elongation at both enhancers and promoters (Kanno et al., 2014), was investigated as a candidate protein for the specific recognition of the H3K27ac mark. BD1 of Brd4 has earlier been reported to bind H3K27ac in a histone peptide SPOT array (Filippakopoulos et al., 2012). H3K27ac and Brd4 have been found to co-localize in enhancer chromatin, and high levels of Brd4 are present at super-enhancers, which also exhibit high levels of H3K27ac (Lovén et al., 2013). The co-localization of Brd4 and H3K27ac, combined with SPOT array data suggesting binding between the two, laid the basis of this work, where potential binding parameters were to be determined by means of histone peptide binding assays, SPR and ITC.

5.1 Histone peptide binding assays show no binding between Brd4 bromodomains and H3K27ac

An interaction between BD1 of Brd4 and H3K27ac had been previously observed in a SPOT- array assay where binding between 33 different human bromodomains and all possible single histone acetylation marks were investigated (Filippakopoulos et al., 2012). In this array, acetylated histone peptides with a length of 10-14 amino acids were synthesized directly on cellulose membranes. His-tagged bromodomains were incubated with the membrane, and after incubation, the bound domains were detected by immunoblotting with anti-His antibodies. Weak binding between BD1 and H3K27ac peptide was detected in one of these binding assays, while another assay detected a strong binding (Filippakopoulos et al., 2012).

The objective of this project was to confirm the binding between Brd4 BD1 and H3K27ac with more quantitative methods, in order to lay the ground for future functional studies.

First, histone peptide binding assays were performed; a method similar to the SPOT array assays used by Filippakopoulos *et al.* (2012). Histone peptide binding assays were carried out with GST-fusion Brd4 bromodomains and a panel of synthetic, biotinylated, modified and non-modified histone peptides. Our results showed, however, no significant binding between GST-BD1 or –BD2 and the H3K27ac peptide (Figure 4.5 A and B). Weak signals were detected for GST-BD1 with H3K27ac, but signals of similar intensities were observed with the negative controls as well, indicating that this was most likely due to unspecific interactions between GST-fusion proteins and the peptide, or between the proteins and the Sepharose beads. Interactions between GST-BD1 and Sepharose beads were detected in one out of three replicates that included this control.

Strong binding between the H4tetra-ac peptide and GST-BD1 was, observed in all replicates, indicating that the domain was functional with capacity to bind other acetylated lysines. Strong binding between H4tetra-ac and GST-BD2 on the other hand was only observed in 1 out of 4 replicates, with large differences in the detected signal intensities. The reason for these large differences is unknown, but was most likely due to technical variations. Previous measurements of the interaction between BD2 of Brd4 and H4tetra-ac peptide by ITC gave a K_D of 26.6 μM for this interaction (Filippakopoulos et al., 2012). In comparison, the same study found a K_D of 2.8 μM for BD1 binding to H4tetra-ac.

This suggests that our assay may not have been sufficiently sensitive to detect a low affinity interaction between the Brd4 bromodomains and H3K27ac. Our histone peptide binding assays were apparently also prone to signals caused by unspecific binding, as pulldown of GST by different peptides was observed in several replicates. As we observed non-specific binding in our initial histone peptide binding assays, we reduced the concentration of bromodomains in our experiments. While a lower concentration of protein in these experiments may have increased the specificity in the assay, it may also have lowered the sensitivity.

Bromodomains have been shown to bind with higher affinity to histone peptides that have two acetyl-lysines separated by 2-5 amino acids (Morinière et al., 2009). In light of this, a di-acetylated peptide (H3K23,K27ac) was also included in the assay. However, no binding was observed between H3K23,K27ac and the Brd4 bromodomains. It has been reported that the number and types of amino acids that separate acetylated lysines affect the binding-specificity of Brd4 BD1 (Filippakopoulos et al., 2012). BD1 was found to prefer acetylated lysines separated by the sequence "GG", as is found between H4 K5 and K8. Positive residues in the sequence were found to diminish binding. The amino acid sequence between H3 K23 and K27 is "AAR", which could explain the lack of binding observed in our assays. Interestingly, none of the lysines of H3 are separated by linker sequences optimal for BD1- binding. Binding by BD2 is less affected by the length and composition of the linker region.

5.2 Lack of binding between Brd4 bromodomains and H3K27 is confirmed by ITC

After our initial histone peptide binding assays indicated that none of the Brd4 bromodomains bind the H3K27ac peptides, we wished to confirm these results by the use of ITC. The molecular interaction between two molecules, at equilibrium in solution, can be measured by ITC. The measurement of heat transfer during binding enables determination of binding constants (K_D), reaction stoichiometry (n), enthalpy and entropy. These parameters give a good biophysical characterization of the binding reaction. In this work, ITC measurements were carried out with His-tagged Brd4 bromodomains and H3K27ac and H4tetra-ac peptides. No apparent binding was observed

between either of the two Brd4 bromodomains and H3K27ac, confirming the observations made from histone peptide binding assays. There were however difficulties with these measurements, as is discussed below.

5.3 His-BD1 binds H4tetra-ac peptide, but not in a simple 1:1 relationship

Measurements with ITC showed binding between His-BD1 and H4tetra-ac with a K_D of 5.3 ± 0.31μM. Previous studies have found an affinity of 2.8 μM using ITC (Filippakopoulos et al.,2012), and 2.4 μM using SPR (Jung et al., 2014), for this interaction. Fitting the data for binding between His-BD1 and H4tetra-ac to a binding model for independent binding sites resulted in a binding curve that lacked the lower plateau of a typical sigmoidal binding model. This is most probably due to the large difference in concentration between His-BD1 and H4tetra-ac peptide. This large concentration difference was used because bromodomains are reported to have low affinities for their acetyl-lysine ligands, which requires that high peptide concentrations are needed for ITC experiments.

A stoichiometry (n-value) of 0.66± 0.11 was calculated from the three ITC replicates of binding between His-BD1 and H4tetra-ac. The n-value represents the number of binding sites on the protein, and a value below 1 could indicate that several domains are binding the same peptide. Aggregation of domains can cause changes in the estimated n-value of a binding reaction, which is likely to be the case for ITC with His-BD1. Interestingly, an n-value of 0.57 for the binding between BD1 and H4tetra-ac has previously been reported, suggesting that the binding mechanism might not be a simple 1:1 binding (Filippakopoulos et al. 2012). A stoichiometry value of 0.5 has also been reported for binding of both BD1 and BD2 of several BET-family proteins to H4 peptides acetylated at three or more positions (Filippakopoulos et al., 2012). This could indicate that two bromodomains bind to each H4tera-ac peptide, perhaps binding two acetyl-lysines each, as is the case for other bromodomains (Morinière et al., 2009). The dimensions of the bromodomains and pairs of acetylated lysines on the tetra-acetylated histone H4 tail are compatible with a model where two bromodomains can bind simultaneously to one and the same histone tail (R. Aasland, pers. comm). In addition, Brd4 BD1 was shown to have higher affinity for H4 histone peptides acetylated at four positions (K5,8,12,16) than for

di-acetylated peptides (H4K5,8ac, H4K8,12ac or H4K12,16ac) (Filippakopoulos et al., 2012). This could indicate that two bromodomains bind to the tetra-acetylated peptide. It is important to keep in mind that these studies were done with free bromodomains, and out of context to the full-length Brd4 protein.

5.4 His-BD2 shows weak binding to H4tetra-ac

ITC with His-BD2 and H4tetra-ac showed signs of weak binding, in the form of heat signals that decreased as more peptide was titrated into the sample cell. When compared to ITC with His-BD2 and H3K27ac (Figure 4.13 A and C), which in this context can serve as a negative control, there is a large difference in the pattern of heat rates. However, the baseline of His-BD2 ITC data was very unstable, and large "bumps" that can be seen close to the injection peaks cause the area data to increase. These "bumps" are most likely due to domain-domain interactions in the sample caused by aggregation. The increase in area under the peaks, combined with the unevenness of the peaks themselves made modeling of the data difficult. Hence no quantitative calculations could be made. Earlier ITC experiments of the binding between BD2 and H4tera-ac found an affinity of 26.6 μM (Filippakopoulos et al., 2012). These experiments, however, used peptide concentrations of 1.5 mM and protein concentrations of 50 μM, whereas our experiments were carried out with 1 mM H4tetra-ac peptide and 40 μM His-BD2. The higher concentrations of peptide and protein in these experiments can explain why the binding could be quantified in these experiments, but not in ours.

5.5 Aggregation of His-tagged bromodomains interfered with ITC

Studies of the oligomeric states of His-BD1 and BD2 with SEC and DLS showed that these domains formed large aggregates shortly after purification. Time course experiments of the size distribution of His-BD1 by DLS showed that it aggregated rapidly, first to a particle with a diameter of 164 nm, and then further into even larger complexes with a hydrodynamic diameter that exceeded 1000 nm. Based on the relation between molecular weight and hydrodynamic radius (Stokes-Einstein radius), the most prominent peak (peak 1 figure 4.9.A) of His-BD1 was estimated to be 40-52 kDa, while the most prominent

peak in His-BD2 was found to be 52 kDa. Lysozyme (13.7 kDa) was by the same method, estimated to be 27.5 kDa. Many factors, including protein concentration, the ionic strength of the solvent and the polydispersity of the sample, can influence the apparent particle diameter in DLS measurements. This value can therefore be considered to be an overestimate. This is supported by data from size exclusion chromatography (SEC) which showed that the major molecule in the His-BD1 sample has a molecular weight of ~13 kDa. This is close to the theoretical molecular weight of His-BD1 (16.3 kDa). Hence, the SEC data suggest that most of the His-BD1 is a monomer in solution. Analysis of the His-BD1 and His-BD2 samples by DLS showed a high degree of polydispersity (PD index= 0.3) and made the analysis of particle sizes in these samples difficult. DLS time course data of His-BD1 showed that larger particles were forming, and confirmed that aggregation was occurring rapidly. Particle size distribution measurements were done in T7.5 buffer, the same buffer used for ITC, at a protein concentration of 214 µM. In ITC experiments, the concentration of His-BD1 and His-BD2 was much lower, at 40 µM, so the rate of aggregation estimated from DLS is not directly applicable. However, the ITC data for His-BD1 and His-BD2 with acetylated histone peptides (Figures 4.12 and 4.13) showed signs of heat-generating interactions that were independent of the titration of peptide into the sample cell. This may be an indication that aggregation was occurring during the experiment. This effect was even more pronounced in experiments with His-BD1 or His-BD2 and H3K27ac peptide, where distinguishing the individual peaks following injections was difficult. The aggregation of His-BD1 in ITC experiments with H4tera-ac resulted in an unstable baseline, which propagated into the modeled area data and caused large deviations in the upper plateau of the sigmoidal curve. This lead to a high degree of uncertainty when the data were fitted to the model, hence, the calculated binding parameters should be interpreted with care.

5.6 Comparison to other binding studies with Brd4 bromodomains

Our experiments with both histone peptide binding assays and ITC showed no binding between Brd4 bromodomains and H3K27ac peptide *in vitro*. This was contrary to previously published data which suggested binding between Brd4 BD1 and H3K27ac (Filippakopoulos et al., 2012). The SPOT assay performed in this study is however a large array where many bromodomains and peptides were screened for binding, and it is likely

that false positives occur in this type of assay. A particular problem in such a high-throughput experiment is that the quality and oligomeric state of each of the proteins may not have been properly monitored. The Brd4 bromodomains utilized in the SPOT assays had the same amino acid sequences as our own (Figure 4.1), but were not reported to aggregate. The data presented here is a strong indication that the data from the SPOT assays must be interpreted with care.

A recent study by Jung *et al.* (2014) showed similar results to ours, where lack of binding between Brd4 bromodomains and H3K27ac was observed using time-resolved fluorescence resonance energy transfer (TR-FRET) (Jung et al., 2014). Even though none of the Brd4 bromodomains showed binding to H3K27ac peptides *in vitro* in our experiments, this might not be directly applicable to a biological setting.

5.7 The role of Brd4 at enhancer and promoter elements

As our results showed that none of the bromodomains of Brd4 bind H3K27ac *in vitro*, the role of Brd4 as a specific H3K27ac-binder in enhancer chromatin must be reconsidered. Previous studies have shown that Brd4 occupancy at enhancers is dependent on its bromodomains, as inhibition with JQ1, a specific BET bromodomain inhibitor, prevents binding of Brd4 to enhancer chromatin (Kanno et al., 2014; Lovén et al., 2013). Brd4 is involved in the regulation of transcription elongation at both promoters and enhancers, and has been shown to mediate eRNA transcription at several active enhancers (Kanno et al., 2014; Lovén et al., 2013; Nagarajan et al., 2014). This action might however not be dependent on recruitment of Brd4 to enhancers through binding to H3K27ac.

Our results showed that none of the bromodomains of Brd4 isolated from the full-length protein bind H3K27ac peptides *in vitro.* The affinity of Brd4 to H3K27ac in living cells might be regulated by the presence of other factors. Many bromodomains show low affinities for acetylated histone peptides *in vitro*, and it is possible that additional factors might contribute to binding *in vivo.* The presence of other nearby marks, such as phosphorylation and methylation has also been reported to affect the affinity of bromodomains to their targets (Filippakopoulos et al., 2012). The two bromodomains of Brd4 might work together or interact with each other in ways that could affect the protein's affinity for specific or combination of acetylation marks. Other regions of Brd4

have been shown to influence its affinity for acetylated chromatin. The NPS-region immediately C-terminal of BD2 (Refer to figure 1.5) can bind BD2 when not phosphorylated, and prevents BD2 from interacting with acetylated chromatin (Wu et al., 2013). Phosphorylation of this region by casein kinase II unmasks BD2 and allows Brd4 to be recruited to acetylated chromatin. Phosphorylation of NPS also allows binding to the transcription factor p53, and subsequent Brd4-mediated recruitment of p53 to target genes and activation of transcription. When Brd4 binds to and cooperates with p53, it takes on a gene-specific regulatory function (Wu et al., 2013).

In recent mass spectroscopy-coupled ChIP experiments, Brd4 was found to be the protein with the highest correlation with H3K27ac in the genome, and was found to be especially predominant at active enhancers (Engelen et al., 2015). These experiments did, however, use an extended cross-linking procedure, which could allow for detection of protein complexes. Co-localization of Brd4 and H3K27ac in chromatin does, however, not necessarily mean that Brd4 or its bromodomains are responsible for binding this mark.

H3K27ac is also not the only acetylation mark present at enhancers, H3K9ac and H3K14ac have also been detected near active enhancers in nine human cell types (H3K9ac) and in mouse embryonic stem cells (H3K9ac and H3K14ac) (Ernst et al., 2011; Karmodiya et al., 2012). It is possible that Brd4 is recruited to enhancer chromatin by binding to other acetyl-lysines in the histone tails, or to acetylated transcription factors. Brd4 has been reported to bind acetylated RelA, a subunit of the transcription factor NFkB through its bromodomains (Carlin et al., 2012). Interactions between the Brd4 bromodomains and transcription factor TWIST have also been reported (Shi et al., 2014). Brd4 might be present in a larger complex of proteins, where other proteins are responsible for the recognition of H3K27ac, and thus the recruitment to active enhancers.

Recent studies have suggested that Brd4 acts as a histone chaperone that assists Pol II elongation through hyper-acetylated chromatin (Kanno et al., 2014). In this study, Brd4 allowed transcription of Pol II through hyper-acetylated nucleosomes in a defined *in vitro* assay which was performed in the absence of P-TEFb. This action of Brd4 was suggested to occur at both promoters and enhancers. This could suggest that Brd4 can regulate transcription independently from P-TEFb and the methyltransferase NSD3 (Rahman et al., 2011).

After the start of this project, the YEATS domain of human AF9, a subunit of the super elongation complex, was found to bind H3K9ac, H3K18ac and H3K27ac with high affinity (Li et al., 2014). The affinity of the YEATS domain for its acetylated targets is higher than that of many bromodomains (Filippakopoulos et al., 2012), which makes it a very interesting candidate for the specific recognition of H3K27ac. Brd4 and AF9 have both been reported to interact with the elongation factor P-TEFb, and it has been suggested that they also both bind and act as transcriptional co-activators of nuclear retinoid receptors (Flajollet et al., 2013). So far, no direct interaction between Brd4 and AF9 has reported.

5.8 Future perspectives

In this study, binding between transcriptional regulator Brd4, and H3K27ac, a histone modification enriched in active enhancers, was investigated. In our binding assays, which included histone peptide binding assays and ITC, no interaction was observed between either of the acetyl-lysine- binding bromodomains of Brd4 and H3K27ac histone peptides. These assays were, however, performed with single bromodomains, and several difficulties arose during the experiments. GST-fusion protein showed high background binding, and His-tagged bromodomains used for ITC measurements were found to aggregate.

In future work, creating new and more soluble constructs would greatly improve the quantitative measurements of binding. In addition, investigation of binding with full-length Brd4, or with protein constructs containing both bromodomains could yield more information of a possible binding between Brd4 and H3K27ac. Also, the chromatin context might play a role in "reader" protein binding, hence using nucleosome arrays as a substrate in binding experiments is advisable.

Even though the investigation of possible binding between Brd4 and H3K27ac can be expanded, it would be of interest to find other binding candidates for the recognition of H3K27ac and determine their role in enhancer-promoter communication. The YEATS domain- containing protein AF9, or the three other human YEATS proteins are good choices for candidate proteins, as the YEATS domain has been shown to bind H3K27ac

with high affinity (Li et al., 2014). Some PHD-fingers have also been reported to bind acetylated lysines (Ali et al., 2012) and could be investigated as candidates.

Pull-down experiments from nuclear extracts with H3K27ac peptides or recombinant nucleosomes carrying H3K27ac (Nguyen et al., 2014) followed by mass spectrometry would be one way to search for the true H3K27ac binders. Such experiments are in progress in our laboratory using an approach based on stable isotope labeling of amino acids in cell culture (SILAC)

6. References

Ali, M., Yan, K., Lalonde, M.-E., Degerny, C., Rothbart, S.B., Strahl, B.D., Côté, J., Yang, X.-J., and Kutateladze, T.G. (2012). Tandem PHD fingers of MORF/MOZ acetyltransferases display selectivity for acetylated histone H3 and are required for the association with chromatin. J. Mol. Biol. *424*, 328–338.

Amano, T., Sagai, T., Tanabe, H., Mizushina, Y., Nakazawa, H., and Shiroishi, T. (2009). Chromosomal dynamics at the Shh locus: limb bud-specific differential regulation of competence and active transcription. Dev. Cell *16*, 47–57.

Andersson, R., Gebhard, C., Miguel-Escalada, I., Hoof, I., Bornholdt, J., Boyd, M., Chen, Y., Zhao, X., Schmidl, C., Suzuki, T., et al. (2014). An atlas of active enhancers across human cell types and tissues. Nature *507*, 455–461.

Armstrong, L. (2014). Epigenetics.

Banerji, J., Rusconi, S., and Schaffner, W. (1981). Expression of a beta-globin gene is enhanced by remote SV40 DNA sequences. Cell *27*, 299–308.

Berger, S.L., Kouzarides, T., Shiekhattar, R., and Shilatifard, A. (2009). An operational definition of epigenetics An operational definition of epigenetics. 781–783.

Bonn, S., Zinzen, R.P., Girardot, C., Gustafson, E.H., Perez-Gonzalez, A., Delhomme, N., Ghavi-Helm, Y., Wilczyński, B., Riddell, A., and Furlong, E.E.M. (2012). Tissue-specific analysis of chromatin state identifies temporal signatures of enhancer activity during embryonic development. Nat. Genet. *44*, 148–156.

Bulger, M., and Groudine, M. (1999). Looping versus linking : toward a model for long-distance gene activation. Genes Dev. 2465–2477.

Bulger, M., and Groudine, M. (2010). Enhancers: The abundance and function of regulatory sequences beyond promoters. Dev. Biol. *339*, 250–257.

Calo, E., and Wysocka, J. (2013). Modification of Enhancer Chromatin: What, How, and Why? Mol. Cell *49*, 825–837.

Carlin, D., Sepich, D., Grover, V.K., Cooper, M.K., Solnica-Krezel, L., and Inbal, A. (2012). Six3 cooperates with Hedgehog signaling to specify ventral telencephalon by promoting early expression of Foxg1a and repressing Wnt signaling. Dev. Cambridge Engl. *139*, 2614–2624.

Cheung, P., Allis, C.D., and Sassone-Corsi, P. (2000). Signaling to Chromatin through Histone Modifications. Cell *103*, 263–271.

Creyghton, M.P., Cheng, A.W., Welstead, G.G., Kooistra, T., Carey, B.W., Steine, E.J., Hanna, J., Lodato, M. a, Frampton, G.M., Sharp, P. a, et al. (2010). Histone H3K27ac separates

active from poised enhancers and predicts developmental state. Proc. Natl. Acad. Sci. U. S. A. *107*, 21931–21936.

Dhalluin, C., Carlson, J.E., Zeng, L., He, C., Aggarwal, a K., and Zhou, M.M. (1999). Structure and ligand of a histone acetyltransferase bromodomain. Nature *399*, 491–496.

Dixon, J.R., Selvaraj, S., Yue, F., Kim, A., Li, Y., Shen, Y., Hu, M., Liu, J.S., and Ren, B. (2012). Topological domains in mammalian genomes identified by analysis of chromatin interactions. Nature *485*, 376–380.

Dunham, I., Kundaje, A., Aldred, S.F., Collins, P.J., Davis, C. a., Doyle, F., Epstein, C.B., Frietze, S., Harrow, J., Kaul, R., et al. (2012). An integrated encyclopedia of DNA elements in the human genome. Nature *489*, 57–74.

Elgin, S.C.R. (1988). The formation and function of DNAase I hypersensitive sites in the process of gene activation. J. Biol. Chem. *263*, 19259–19262.

Engelen, E., Brandsma, J.H., Moen, M.J., Signorile, L., Dekkers, D.H.W., Demmers, J., Kockx, C.E.M., Ozgür, Z., van IJcken, W.F.J., van den Berg, D.L.C., et al. (2015). Proteins that bind regulatory regions identified by histone modification chromatin immunoprecipitations and mass spectrometry. Nat. Commun. *6*, 7155.

Ernst, J., and Kellis, M. (2010). Discovery and characterization of chromatin states for systematic annotation of the human genome. Nat. Biotechnol. *28*, 817–825.

Ernst, J., Kheradpour, P., Mikkelsen, T.S., Shoresh, N., Ward, L.D., Epstein, C.B., Zhang, X., Wang, L., Issner, R., Coyne, M., et al. (2011). Mapping and analysis of chromatin state dynamics in nine human cell types. Nature *473*, 43–49.

Filippakopoulos, P., Picaud, S., Mangos, M., Keates, T., Lambert, J.-P., Barsyte-Lovejoy, D., Felletar, I., Volkmer, R., Müller, S., Pawson, T., et al. (2012). Histone recognition and large-scale structural analysis of the human bromodomain family. Cell *149*, 214–231.

Flajollet, S., Rachez, C., Ploton, M., Schulz, C., Gallais, R., Métivier, R., Pawlak, M., Leray, A., Issulahi, A.A., Héliot, L., et al. (2013). The Elongation Complex Components BRD4 and MLLT3/AF9 Are Transcriptional Coactivators of Nuclear Retinoid Receptors. PLoS One *8*.

Florence, B., and Faller, D. V (2001). You bet-cha: a novel family of transcriptional regulators. Front. Biosci. *6*, D1008–D1018.

Freire, E., Mayorga, O., and Straume, M. (1990). Isothermal Titration. Anal. Chem. *62*.

Ghavi-Helm, Y., Klein, F.A., Pakozdi, T., Ciglar, L., Noordermeer, D., Huber, W., and Furlong, E.E.M. (2014). Enhancer loops appear stable during development and are associated with paused polymerase. Nature.

Grewal, S.I.S., and Jia, S. (2007). Heterochromatin revisited. Nat. Rev. Genet. *8*, 35–46.

Grunstein, M. (1997). Histone acetylation in chromatin structure and transcription. Nature *389*, 349–352.

Heintzman, N.D., Stuart, R.K., Hon, G., Fu, Y., Ching, C.W., Hawkins, R.D., Barrera, L.O., Van Calcar, S., Qu, C., Ching, K. a, et al. (2007). Distinct and predictive chromatin signatures of transcriptional promoters and enhancers in the human genome. Nat. Genet. *39*, 311–318.

Heintzman, N.D., Hon, G.C., Hawkins, R.D., Kheradpour, P., Stark, A., Harp, L.F., Ye, Z., Lee, L.K., Stuart, R.K., Ching, C.W., et al. (2009). Histone modifications at human enhancers reflect global cell-type-specific gene expression. Nature *459*, 108–112.

Heinz, S., Romanoski, C.E., Benner, C., and Glass, C.K. (2015). The selection and function of cell type-specific enhancers. Nat. Rev. Mol. Cell Biol. *16*, 144–154.

Hong, P., Koza, S., and Bouvier, E.S.P. (2012). Size-Exclusion Chromatography for the Analysis of Protein Biotherapeutics and their Aggregates. J. Liq. Chromatogr. Relat. Technol. *35*, 2923–2950.

Houzelstein, D., Bullock, S.L., Lynch, D.E., Grigorieva, E.F., Wilson, V.A., and Beddington, R.S.P. (2002). Growth and early postimplantation defects in mice deficient for the bromodomain-containing protein Brd4. Mol. Cell. Biol. *22*, 3794–3802.

Instruments, M. (2011). Dynamic Light Scattering, Common Terms Defined. 1–6.

Jiang, Y.W., Veschambre, P., Erdjument-Bromage, H., Tempst, P., Conaway, J.W., Conaway, R.C., and Kornberg, R.D. (1998). Mammalian mediator of transcriptional regulation and its possible role as an end-point of signal transduction pathways. Proc. Natl. Acad. Sci. U. S. A. *95*, 8538–8543.

Jin, F., Li, Y., Dixon, J.R., Selvaraj, S., Ye, Z., Lee, A.Y., Yen, C.-A., Schmitt, A.D., Espinoza, C. a, and Ren, B. (2013). A high-resolution map of the three-dimensional chromatin interactome in human cells. Nature *503*, 290–294.

Jung, M., Philpott, M., Müller, S., Schulze, J., Badock, V., Eberspächer, U., Moosmayer, D., Bader, B., Schmees, N., Fernández-Montalván, A., et al. (2014). Affinity map of bromodomain protein 4 (BRD4) interactions with the histone H4 tail and the small molecule inhibitor JQ1. J. Biol. Chem. *289*, 9304–9319.

Kanno, T., Kanno, Y., Leroy, G., Campos, E., Sun, H., Brooks, S.R., Vahedi, G., Heightman, T.D., Garcia, B.A., Reinberg, D., et al. (2014). BRD4 assists elongation of both coding and enhancer RNAs by interacting with acetylated histones. Nat. Struct. & Mol. Biol. *21*, 1047–1057.

Karmodiya, K., Krebs, A.R., Oulad-Abdelghani, M., Kimura, H., and Tora, L. (2012). H3K9 and H3K14 acetylation co-occur at many gene regulatory elements, while H3K14ac marks a subset of inactive inducible promoters in mouse embryonic stem cells. BMC Genomics *13*, 424.

Kim, T.-K., Hemberg, M., Gray, J.M., Costa, A.M., Bear, D.M., Wu, J., Harmin, D. a, Laptewicz, M., Barbara-Haley, K., Kuersten, S., et al. (2010). Widespread transcription at neuronal activity-regulated enhancers. Nature *465*, 182–187.

Kouzarides, T. (2000). Acetylation: a regulatory modi cation to rival phosphorylation? EMBO J. *19*, 1176–1179.

Kouzarides, T. (2007). Chromatin Modifications and Their Function. Cell *128*, 693–705.

De Laat, W., and Duboule, D. (2013). Topology of mammalian developmental enhancers and their regulatory landscapes. Nature *502*, 499–506.

Lam, M.T.Y., Li, W., Rosenfeld, M.G., and Glass, C.K. (2014). Enhancer RNAs and regulated transcriptional programs. Trends Biochem. Sci. *39*, 170–182.

Leavitt, S., and Freire, E. (2001). Direct measurement of protein binding energetics by isothermal titration calorimetry. Curr. Opin. Struct. Biol. *11*, 560–566.

Li, Y., Wen, H., Xi, Y., Tanaka, K., Wang, H., Peng, D., Ren, Y., Jin, Q., Dent, S.Y.R., Li, W., et al. (2014). AF9 YEATS Domain Links Histone Acetylation to DOT1L-Mediated H3K79 Methylation. Cell *159*, 558–571.

Liu, W., Ma, Q., Wong, K., Li, W., Ohgi, K., Zhang, J., Aggarwal, A.K., and Rosenfeld, M.G. (2013). Brd4 and JMJD6-Associated Anti-Pause Enhancers in Regulation of Transcriptional Pause Release. Cell *155*, 1581–1595.

Lovén, J., Hoke, H. a., Lin, C.Y., Lau, A., Orlando, D. a., Vakoc, C.R., Bradner, J.E., Lee, T.I., and Young, R. a. (2013). Selective inhibition of tumor oncogenes by disruption of super-enhancers. Cell *153*, 320–334.

Luger, K., Mäder, a W., Richmond, R.K., Sargent, D.F., and Richmond, T.J. (1997). Crystal structure of the nucleosome core particle at 2.8 A resolution. Nature *389*, 251–260.

Moon, K.J., Mochizuki, K., Zhou, M., Jeong, H.S., Brady, J.N., and Ozato, K. (2005). The bromodomain protein Brd4 is a positive regulatory component of P-TEFb and stimulates RNA polymerase II-dependent transcription. Mol. Cell *19*, 523–534.

Morinière, J., Rousseaux, S., Steuerwald, U., Soler-López, M., Curtet, S., Vitte, A.-L., Govin, J., Gaucher, J., Sadoul, K., Hart, D.J., et al. (2009). Cooperative binding of two acetylation marks on a histone tail by a single bromodomain. Nature *461*, 664–668.

Nagarajan, S., Hossan, T., Alawi, M., Najafova, Z., Indenbirken, D., Bedi, U., Taipaleenmäki, H., Ben-Batalla, I., Scheller, M., Loges, S., et al. (2014). Bromodomain Protein BRD4 Is Required for Estrogen Receptor-Dependent Enhancer Activation and Gene Transcription. Cell Rep. *4*.

Nakamura, Y., Umehara, T., Nakano, K., Moon, K.J., Shirouzu, M., Morita, S., Uda-Tochio, H., Hamana, H., Terada, T., Adachi, N., et al. (2007). Crystal structure of the human BRD2

bromodomain: Insights into dimerization and recognition of acetylated histone H4. J. Biol. Chem. *282*, 4193–4201.

Nguyen, U.T.T., Bittova, L., Müller, M.M., Fierz, B., David, Y., Houck-Loomis, B., Feng, V., Dann, G.P., and Muir, T.W. (2014). Accelerated chromatin biochemistry using DNA-barcoded nucleosome libraries. Nat. Methods *11*, 834–840.

Nygren, P.-Å., Stefan, S., and Uhlén, M. (1994). Engineering proteins to facilitate bioprocessing. Trends Biotechnol. *12*, 184–188.

Oki, M., Aihara, H., and Ito, T. (2007). Role of histone phosphorylation in chromatin dynamics and its implications in diseases. Subcell. Biochem. *41*, 319–336.

Peng, J., Liu, M., Marion, J., Zhu, Y., and Price, D.H. (1998). RNA polymerase II elongation control. Cold Spring Harb. Symp. Quant. Biol. *63*, 365–370.

Perla Cota, M.S. and D.E.R. (2013). Stem Cells and Epigenetic Reprogramming. In Pluripotent Stem Cells, pp. 179–204.

Pertea, M., and Salzberg, S.L. (2010). Between a chicken and a grape: estimating the number of human genes. Genome Biol. *11*, 206.

Plank, J.L., and Dean, A. (2014). Enhancer function: Mechanistic and genome-wide insights come together. Mol. Cell *55*, 5–14.

Prasanth, K. V, Camiolo, M., Chan, G., Tripathi, V., Denis, L., Nakamura, T., Hübner, M.R., and Spector, D.L. (2010). Nuclear organization and dynamics of 7SK RNA in regulating gene expression. Mol. Biol. Cell *21*, 4184–4196.

Rack, J.G.M., Lutter, T., Kjæreng Bjerga, G.E., Guder, C., Ehrhardt, C., Värv, S., Ziegler, M., and Aasland, R. (2014). The PHD finger of p300 influences its ability to acetylate histone and non-histone targets. J. Mol. Biol. *426*, 3960–3972.

Rada-Iglesias, A., Bajpai, R., Swigut, T., Brugmann, S.A., Flynn, R.A., and Wysocka, J. (2011). A unique chromatin signature uncovers early developmental enhancers in humans. Nature *470*, 279–283.

Ragvin, A., Valvatne, H., Erdal, S., Årskog, V., Tufteland, K.R., Breen, K., Øyan, A.M., Eberharter, A., Gibson, T.J., Becker, P.B., et al. (2004). Nucleosome binding by the bromodomain and PHD finger of the transcriptional cofactor p300. J. Mol. Biol. *337*, 773–788.

Rahman, S., Sowa, M.E., Ottinger, M., Smith, J. a, Shi, Y., Harper, J.W., and Howley, P.M. (2011). The Brd4 extraterminal domain confers transcription activation independent of pTEFb by recruiting multiple proteins, including NSD3. Mol. Cell. Biol. *31*, 2641–2652.

Rao, S.S.P., Huntley, M.H., Durand, N.C., and Stamenova, E.K. (2014). A 3D Map of the Human Genome at Kilobase Resolution Reveals Principles of Chromatin Looping. Cell *159*, 1665–1680.

Raynaud, C., Mallory, A.C., Latrasse, D., Jégu, T., Bruggeman, Q., Delarue, M., Bergounioux, C., and Benhamed, M. (2014). Chromatin meets the cell cycle. J. Exp. Bot. *65*, 2677–2689.

Ruthenburg, A.J., Li, H., Patel, D.J., and Allis, C.D. (2007). Multivalent engagement of chromatin modifications by linked binding modules. Nat. Rev. Mol. Cell Biol. *8*, 983–994.

Sadakierska-Chudy, A., and Filip, M. (2014). A Comprehensive View of the Epigenetic Landscape. Part II: Histone Post-translational Modification, Nucleosome Level, and Chromatin Regulation by ncRNAs. Neurotox. Res. *27*, 172–197.

De Santa, F., Barozzi, I., Mietton, F., Ghisletti, S., Polletti, S., Tusi, B.K., Muller, H., Ragoussis, J., Wei, C.L., and Natoli, G. (2010). A large fraction of extragenic RNA Pol II transcription sites overlap enhancers. PLoS Biol. *8*.

Schröder, S., Cho, S., Zeng, L., Zhang, Q., Kaehlcke, K., Mak, L., Lau, J., Bisgrove, D., Schnölzer, M., Verdin, E., et al. (2012). Two-pronged binding with bromodomain-containing protein 4 liberates positive transcription elongation factor b from inactive ribonucleoprotein complexes. J. Biol. Chem. *287*, 1090–1099.

Shahbazian, M.D., and Grunstein, M. (2007). Functions of site-specific histone acetylation and deacetylation. Annu. Rev. Biochem. *76*, 75–100.

Shi, J., and Vakoc, C.R. (2014). The mechanisms behind the therapeutic activity of BET bromodomain inhibition. Mol. Cell *54*, 728–736.

Shi, J., Wang, Y., Zeng, L., Wu, Y., Deng, J., Zhang, Q., Lin, Y., Li, J., Kang, T., Tao, M., et al. (2014). Disrupting the interaction of BRD4 with diacetylated Twist suppresses tumorigenesis in basal-like breast cancer. Cancer Cell *25*, 210–225.

Shi, X., Hong, T., Walter, K.L., Ewalt, M., Michishita, E., Hung, T., Carney, D., Peña, P., Lan, F., Kaadige, M.R., et al. (2006). ING2 PHD domain links histone H3 lysine 4 methylation to active gene repression. Nature *442*, 96–99.

Shiio, Y., and Eisenman, R.N. (2003). Histone sumoylation is associated with transcriptional repression. Proc. Natl. Acad. Sci. U. S. A. *100*, 13225–13230.

Shlyueva, D., Stampfel, G., and Stark, A. (2014). Transcriptional enhancers: from properties to genome-wide predictions. Nat. Rev. Genet. *15*, 272–286.

Strahl, B.D., and Allis, C.D. (2000). The language of covalent histone modifications. Nature *403*, 41–45.

Strahl, B.D., Ohba, R., Cook, R.G., and Allis, C.D. (1999). Methylation of histone H3 at lysine 4 is highly conserved and correlates with transcriptionally active nuclei in Tetrahymena. Proc. Natl. Acad. Sci. U. S. A. *96*, 14967–14972.

Struhl, K. (1998). Histone acetylation and transcriptional regulatory mechanisms. Genes Dev. *12*, 599–606.

Su, D., Hu, Q., Li, Q., Thompson, J.R., Cui, G., Fazly, A., Davies, B.A., Botuyan, M.V., Zhang, Z., and Mer, G. (2012). Structural basis for recognition of H3K56-acetylated histone H3-H4 by the chaperone Rtt106. Nature *483*, 104–107.

Tan, M., Luo, H., Lee, S., Jin, F., Yang, J.S., Montellier, E., Buchou, T., Cheng, Z., Rousseaux, S., Rajagopal, N., et al. (2011). Identification of 67 histone marks and histone lysine crotonylation as a new type of histone modification. Cell *146*, 1016–1028.

Tie, F., Banerjee, R., Stratton, C.A., Prasad-Sinha, J., Stepanik, V., Zlobin, A., Diaz, M.O., Scacheri, P.C., and Harte, P.J. (2009). CBP-mediated acetylation of histone H3 lysine 27 antagonizes Drosophila Polycomb silencing. Development *136*, 3131–3141.

Trojer, P., and Reinberg, D. (2007). Facultative heterochromatin: is there a distinctive molecular signature? Mol. Cell *28*, 1–13.

Venturoli, D., and Rippe, B. (2005). Ficoll and dextran vs. globular proteins as probes for testing glomerular permselectivity: effects of molecular size, shape, charge, and deformability. Am. J. Physiol. Renal Physiol. *288*, F605–F613.

Whyte, W. a., Orlando, D. a., Hnisz, D., Abraham, B.J., Lin, C.Y., Kagey, M.H., Rahl, P.B., Lee, T.I., and Young, R. a. (2013). Master transcription factors and mediator establish super-enhancers at key cell identity genes. Cell *153*, 307–319.

Wu, S.-Y.Y., and Chiang, C.-M.M. (2007). The double bromodomain-containing chromatin adaptor Brd4 and transcriptional regulation. J. Biol. Chem. *282*, 13141–13145.

Wu, S.Y., Lee, a. Y., Lai, H.T., Zhang, H., and Chiang, C.M. (2013). Phospho switch triggers brd4 chromatin binding and activator recruitment for gene-specific targeting. Mol. Cell *49*, 843–857.

Wyatt Technology (2015). Introduction to Light Scattering Theory.

Xi, H., Shulha, H.P., Lin, J.M., Vales, T.R., Fu, Y., Bodine, D.M., McKay, R.D.G., Chenoweth, J.G., Tesar, P.J., Furey, T.S., et al. (2007). Identification and characterization of cell type-specific and ubiquitous chromatin regulatory structures in the human genome. PLoS Genet. *3*, 1377–1388.

Zhang, Y. (2003). Transcriptional regulation by histone ubiquitination and deubiquitination. Genes Dev. *17*, 2733–2740.

Zhang, W., Prakash, C., Sum, C., Gong, Y., Li, Y., Kwok, J.J.T., Thiessen, N., Pettersson, S., Jones, S.J.M., Knapp, S., et al. (2012). Bromodomain-containing protein 4 (BRD4) regulates RNA polymerase II serine 2 phosphorylation in human CD4+ T cells. J. Biol. Chem. *287*, 43137–43155.

7. Appendix

Plasmid map of expression vectors pSXG and pQE30.